Pacific climate reflected in Waipuna Cave dripwater hydrochemistry

Cinthya Nava-Fernandez[1], Adam Hartland[2], Fernando Gázquez[3], Ola Kwiecien[1], Norbert Marwan[4], Bethany Fox[5,2], John Hellstrom[6], Andrew Pearson[2], Brittany Ward[2], Amanda French[2], David A. Hodell[7], Adrian Immenhauser[1], Sebastian F.M. Breitenbach[1]

[1]Sediment- and Isotope Geology, Institute for Geology, Mineralogy and Geophysics, Ruhr-Universität Bochum, Universitätsstr. 150, 44801 Bochum, Germany
[2]Environmental Research Institute, School of Science, Faculty of Science and Engineering, University of Waikato, Hamilton, Waikato, New Zealand
[3]Department of Biology and Geology, Universidad de Almeria, Almería, 04120, Spain
[4]Potsdam Institute for Climate Impact Research (PIK), Member of the Leibniz Association, Potsdam, Germany
[5]Department of Biological and Geographical Sciences, School of Applied Sciences, University of Huddersfield, Queensgate, Huddersfield, UK
[6]School of Earth Sciences, The University of Melbourne, Australia
[7]Godwin Laboratory for Palaeoclimate Research, Department of Earth Sciences, University of Cambridge, Downing Street, Cambridge CB2 3EQ, UK

Correspondence to: Cinthya Nava (cinthya.navafernandez@rub.de)

Abstract

Cave microclimatic and geochemical monitoring is vitally important for correct interpretations of proxy time series from speleothems with regard to past climatic and environmental dynamics. We present results of a comprehensive cave monitoring programme in Waipuna Cave in the North Island of New Zealand, a region that is strongly influenced by the southern Westerlies and the El Niño-Southern Oscillation (ENSO). This study aims to characterise the response of the Waipuna Cave hydrological system to atmospheric circulation dynamics in the southwestern Pacific region in order to verify the quality of ongoing palaeo-environmental reconstructions from this cave.

Dripwater from 10 drip sites was collected at roughly monthly intervals for a period of ca. 3 years for isotopic ($\delta^{18}O$, δD, d-excess, $\delta^{17}O$, $^{17}O_{excess}$) and elemental (Mg/Ca, Sr/Ca) analysis. The monitoring included spot measurements of drip rates, and cave air CO_2 concentration. Cave air temperature and drip rates were also continuously recorded by automatic loggers. These datasets were compared to surface air temperature, rainfall, and potential evaporation from nearby meteorological stations to test the degree of signal transfer and expression of surface environmental conditions in Waipuna Cave hydrochemistry.

Based on the drip response dynamics to rainfall and other characteristics we identified three types of discharge associated with hydrological routing in Waipuna Cave: i) type 1: diffuse flow, ii) type 2: fracture flow, and iii) type 3: combined flow. Dripwater isotopes do not reflect seasonal variability but show higher values during severe drought. Dripwater $\delta^{18}O$ values are characterised by small variability and reflect the mean isotopic signature of precipitation, testifying to rapid and thorough homogenization in the epikarst. Mg/Ca and Sr/Ca ratios in dripwaters are predominantly controlled by prior calcite precipitation (PCP). Prior calcite precipitation is strongest during austral summer (December-February), reflecting drier conditions and lack of effective infiltration, and is weakest during the wet austral winter (July–September). The Sr/Ca ratio is particularly sensitive to ENSO conditions due to the interplay of congruent/incongruent host rock dissolution, which manifests itself in lower Sr/Ca in above-average warmer and wetter (La Niña-like) conditions. Our microclimatic observations at Waipuna Cave provide a valuable baseline for rigorous interpretation of speleothem proxy records aiming at reconstructing the past expression of Pacific climate modes.

1 Introduction

The southwestern fringe of the Pacific Ocean between 30º and 40ºS marks the transition zone between the tropical Pacific and the sub-tropical Southern Ocean. This region's position near the boundary of two markedly different climates makes the southwestern Pacific a key site to capture the signatures of the coupled atmosphere-ocean climate subsystems of the El Niño-Southern-Oscillation (ENSO) and the southern Westerlies (Basher, 1998; Shulmeister et al., 2004). The mid-latitude westerlies are a dominant feature in Southern Hemisphere general circulation. The prevailing wind flow from west to east over Aotearoa New Zealand is present throughout the year but shows maximum intensity in winter (Sturman and Tapper 2014). The westerly circulation has a significant impact on mean rainfall in New Zealand, with strong wind circulation bringing more rainfall to the western parts of the islands (Griffiths, 2006). The effects of both these circulation features are well expressed in seasonal to multi-annual climate variability in New Zealand (Mullan, 1995). New Zealand's climate is strongly modulated by both ENSO and the southern Westerlies, and its agricultural economy reacts sensitively to inter-annual fluctuations in weather patterns caused by their dynamics (Basher, 1998).

During El Niño events, New Zealand is susceptible to increases in the frequency and intensity of westerly and southwesterly winds, accompanied by decreased rainfall in the North Island (Ummenhofer et al., 2007). In contrast, La Niña events are accompanied by stronger northeasterly winds and increased rainfall in the North Island (Griffiths, 2007; Ummenhofer et al., 2007). The link between ENSO events and climate on the west coast of the North Island of New Zealand is reflected in the correlation between precipitation datasets (e.g. the New Plymouth rainfall dataset 1950-2004) and the Nino 3.4 and SOI indices. Rainfall in this area is negatively correlated with Nino 3.4 for the months June to November, indicating that during El Niño events New Plymouth receives below average rainfall in austral winter. The SOI index shows a fairly strong correlation with austral winter rainfall (July to November). During times of positive SOI values, indicative of La Niña, higher than normal precipitation is observed at the west coast (https://climexp.knmi.nl/start.cgi).

The environmental and economic impacts of strong ENSO events for New Zealand are considerable. For example, the severe drought triggered by the strong El Niño event of 1997–1998 caused economic losses of ca. 1 billion NZD (Basher, 1998). The projected effects of ENSO on New Zealand hydroclimate are based on observations of El Niño and La Niña dynamics recorded over the instrumental period. However, such observations cover only a comparatively short time span (beginning early 1800s). The study of the long-term natural variability of New Zealand hydroclimate (and emergent teleconnection patterns) is a priority, both because of the effects of ENSO variability on local economic conditions and because records from this region are sparse but vital for improving the robustness of model projections of future ENSO conditions. Prior to building robust palaeoclimate (ENSO) reconstructions (e.g. by using speleothems), field sites that are highly susceptible to ENSO-related environmental changes must be identified through monitoring campaigns.

Speleothems (secondary cave carbonates) offer precise chronological control and a wide range of environmentally-sensitive proxies, including growth rate, carbon and oxygen isotopes ($\delta^{13}C$, $\delta^{18}O$), major and trace elements, and increasingly, non-traditional isotope systems such as $\delta^{44}Ca$ (Henderson, 2006; Fairchild and Baker 2012; Owen et al., 2016; Magiera et al., 2019) or $\delta^{26}Mg$ (Immenhauser et al., 2010; Riechelmann et al., 2012).

Over the last two decades, speleothems have provided invaluable reconstructions of past rainfall, changes in vegetation, and coupled atmosphere-ocean dynamics (Dorale et al., 1998; Asmerom et al., 2010; Myers et al., 2015; Chen et al., 2016; Griffiths et al., 2016; Lechleitner et al., 2017; Kaushal et al., 2018). Speleothems provide reliable continental palaeoclimate records because they allow for modern calibrations linking palaeo-data from stalagmites with meteorological and direct in-cave monitoring, thus making it possible to trace climatic signals from the surface to the speleothem at timescales from seasonal (Frappier et al., 2002) to orbital (Wang et al., 2001 and Wang et al., 2008; Meckler et al., 2012; Chen et al., 2016). Apart from established methods, ongoing investigations are exploring the use of triple oxygen isotopes (i.e. $^{17}O_{excess}$; see section 3.4 for definition) in carbonate and fluid inclusions in speleothems as a proxy for changes in atmospheric humidity (Affolter et al., 2015, Sha et al., 2020). In rainfall - and presumably in cave dripwater - $^{17}O_{excess}$ mostly reflects the relative humidity during

formation of water vapour at the moisture source (i.e. ocean surface), with temperature having a minor effect (Uechi and Uemura, 2019).

Monitoring of modern cave environments, encompassing ventilation, hydrology and hydrochemistry, is critical for reliable interpretations of palaeo-environmental proxies preserved in speleothems because numerous studies have shown imperfect replication between coeval stalagmites, as well as differences in dripwater composition (McDermott, 2004; Fairchild et al., 2006a; Breitenbach et al., 2015). Some of the key parameters affecting a speleothem's fidelity as an environmental archive include cave air and water temperature, drip discharge dynamics, and cave air pCO_2, as well as dripwater chemistry (Fairchild and Baker, 2012; Tremaine et al., 2016). Analysis of the latter allows a distinction to be made between the processes involved in the transfer of the external environmental signals (e.g., precipitation history, temperature, or soil dynamics) and the processes inherent to the epikarst and cave (e.g. degree of water-rock interaction, seepage-water CO_2 degassing, cave air CO_2 dynamics and prior carbonate precipitation; Oster et al., 2012; Fairchild and Baker, 2012).

The characterization of infiltration pathways is an essential prerequisite for delineating the processes that can modulate dripwater chemistry, i.e. the degree of water-rock interaction taking place in the epikarst and the climate signal transferred by the dripwater to the speleothems. The climatic signal transferred to speleothems can vary even between speleothems from the same chamber, which emphasizes the need for detailed monitoring. As every stalagmite records the conditions that occur in the epikarst, which signals transferred by the feeding dripwater, an in-depth understanding of the forcing mechanisms is vital to understand the differences between non-replicating records.

The physical proprieties of the karst zone define the different levels of porosity (Ford and Williams, 2007). Primary porosity is a matrix of inter-granular pore space, secondary porosity is associated with joints and fractures, and tertiary porosity with solution-enhanced conduits. Seepage water experiences one or a combination of these different porosity types, which determine hydrological pathways (Fairchild and Baker 2012). Conceptual models of cave dripwater hydrology have traditionally sought to delineate these different types of flow routing on the basis of peak discharge and discharge variability. Smart and Friederich (1987), later modified by Baker et al. (1997). More recently, Jex et al. (2012), Markowska et al. (2015), and Mahmud et al. (2018) proposed new classification systems based on long-term drip discharge time series, statistical tests, and clustering models. These site-specific classification systems argue that drip discharge characterisation enables a better understanding of the controls on stalagmite growth and of climate proxies such as stable isotopes and trace metals.

Flow routing to speleothem drip points is the first-order control on dripwater hydrochemistry, with particular relevance for trace elements and other proxies of prior calcite precipitation (PCP) (Fairchild et al., 2000; Wassenburg et al., 2012). PCP serves as a proxy system for moisture availability (Magiera et al., 2019), as it controls the distribution of trace elements in the infiltrating water during precipitation of carbonate depending on their partition coefficient prior to arrival at a stalagmite. During the dry season, when the epikarst is less water-filled, PCP can occur, resulting in an increase in X/Ca ratios in solution (and subsequently the speleothem), while during the wet season, when the epikarst is refilled, PCP is suppressed and dripwater X/Ca ratios are lowered (Fairchild et al. 2009). Common PCP proxy systems include the Group II alkaline earth metals (Mg, Sr, Ba) and stable Ca isotopes ($\delta^{44}Ca$) (Magiera et al., 2019; Owen et al., 2016). Calcium isotopes show particular potential for future quantitative PCP reconstructions. However, linking PCP to rainfall amount requires careful site-specific monitoring and calibration (Li et al., 2018).

Cave monitoring studies in tropical and southwestern Pacific regions have documented strong ENSO signals in Australia (Tadros et al., 2016), Borneo (Moerman et al., 2014) and on Niue Island in the central Pacific (Tremaine et al., 2016). In New Zealand, however, the number of comparable monitoring studies is still limited. Williams and Fowler (2002) investigated the relationship between the oxygen isotope composition of rainfall and dripwater in Aranui Cave (Waitomo region, North Island). They found that neither the seasonal variability nor the ENSO-related variability detected in $\delta^{18}O$ values of rainfall was transferred to the cave dripwaters. In the case of Aranui Cave, this seems to result from homogenization of the water isotope

signal on its path through the soil and epikarst (Williams and Fowler, 2002). These results highlight the importance of understanding local settings and indicate a need for revisiting other New Zealand cave systems in order to test the relationship between external environmental signals and those inherent to the epikarst and cave system.

We hypothesize that the hydrochemistry of Waipuna Cave is sensitive to changes in precipitation patterns, and thus to seasonal variations and dynamics related to ENSO and the southern Westerlies, due to its geographical position and geometry. Our study aims to test this hypothesis through a 3-year cave monitoring study, including measurements of cave ventilation, dripwater hydrochemistry, and local temperature patterns. Our study has three consecutive objectives: i) characterisation of the dripwater chemistry, including major and trace elements (Mg/Ca and Sr/Ca) and isotope geochemistry ($\delta^{17}O$, $\delta^{18}O$, δD, d-excess and $^{17}O_{excess}$); ii) identification of the mechanisms controlling dripwater chemistry; and iii) understanding the relationship between dripwater chemistry and variations in precipitation, with special reference to seasonal and interannual (ENSO) climate conditions.

2 Study area

2.1 Geographical and climatological setting

Waipuna Cave is located in the Waitomo district, North Island, New Zealand (S 38°18'41.3'', E 175°1'14.3'', 395 m above sea level), ca. 27 km from the west coast (Fig. 1a). The Waipuna Cave is a ca. 3.5 km long river cave developed in the clay-rich, stylobedded Oligocene Pancake Limestone (Nelson, 1973, Fig. 1b). The estimated bedrock overburden is ca. 20–30 m. The main passage is accessed via a ca. 25 meter-deep doline. An underground stream flowing through the cave connects a number of larger chambers (Fig. 1c, d). The winding and narrow passage that connects the main chambers limits cave air flow, and the cave atmosphere is relatively isolated from the surface conditions (Fig. 1c). The surface morphology around Waipuna Cave is characterised by a craggy karst landscape with frequent large dolines (Fig. 1b).

The soil zone is generally > 1 m thick typic orthic allophanic (LO) developed on extensive and exceptionally well drained North Island rhyolitic volcanic ash deposits (Hewitt, 2010). The vegetation cover is a patchwork of lush podocarp-hardwood forest with a dense undergrowth of shrubs, ferns, and tree-ferns. This is surrounded by grassland pasture used for grazing cattle. Based on data from Te Kuiti High School, a meteorological station in the Waitomo district, the average conditions during the period from 1950 to 2000 AD include annual rainfall of 1539 mm without any distinct rainy season. Summer and winter monthly precipitation means are similar (95 mm and 150 mm, respectively), with highest values in austral winter (July) and lowest values during austral summer (February). The mean annual temperature is 13.4°C, ranging from an average of 18.5°C in summer to 8°C in winter.

3 Methods

3.1 External environmental monitoring

Several meteorological datasets were used to constrain the relationship between surface and in-cave environmental conditions. A HOBO temperature logger (ONSET, Bourne, Massachusetts) with a precision of ± 0.2°C housed in a purpose-built meteorological station, was deployed a few hundred meters from the cave entrance and recorded air temperature at half-hourly intervals between June 2017 and May 2018, from which daily means were calculated. The same station recorded daily rainfall over the periods April 2016 to September 2016 and May 2017 to May 2018. Rainfall was recorded with a precision of 0.1 mm using a combination of Campbell-Scientific (established in September 2016) and HOBO tipping-bucket rain gauges (established May 2017). Due to technical difficulties, it was not feasible to collect rainfall data over the entire monitoring period. To complement the local meteorological dataset, daily rainfall and potential evapotranspiration (PET, based on the Priestley-Taylor equation) data were obtained from the NIWA National Database (www.clifo.niwa.co.nz) using proximal stations at Otorohanga Glenbrook and Te Kuiti Ews, 22 km and 13 km from Waipuna Cave, respectively.

3.2 Cave environment monitoring

Waipuna Cave was visited at ca. monthly intervals for a period of almost 3 years from April 2016 to February 2019 (32 visits in total). Discrete cave air pCO_2 measurements were conducted during each visit in the sampling chamber using a Vaisala M170 GMP 343 Carbocap CO_2 probe with a precision of ±1 %. These measurements were always conducted before all team members entered the cave chamber to avoid contamination. Water temperature, pH, and electrical conductivity were manually measured on the dripwaters using LAQUAtwin pH and conductivity probes (HORIBA Scientific Japan) calibrated prior to each sampling event. Air temperature in the Organ Loft was recorded every 30 minutes throughout the monitoring period using an automatic HOBO logger.

3.3 Cave water collection and drip rates

Ten drip sites, along with the cave stream, were sampled for water isotopes and elemental concentrations. Seven of the drip sites (WP 1-1, WP 1-2, WP 1-3, WP 1-4, WP-1A, WP 1B and WP-FB) feed a flowstone (Fig. 2a, b). Three further drip sites (WP-2, WP-3 and WP-4) are located a few meters apart below active stalactites (Fig. 2c) on an elevated section within the same chamber, and higher in the ceiling than the first seven drip sites. Additional water samples from the cave stream were also collected (one per visit). Dripwater samples for stable isotope analysis ($\delta^{17}O$, $\delta^{18}O$ and δD) were collected and stored in sterile 2 ml or 10 ml polypropylene bottles, filled with no head space and sealed using laboratory film. Water samples for trace element analysis were collected in 15 ml polypropylene (Falcon) tubes, previously demonstrated to have low metal blanks (Hartland et al., 2015). These samples were acidified with 2 % HNO_3 (using in-house, double Teflon-distilled acid) and refrigerated until analysis.

Drip rates at the monitored sites were determined using two independent methods. First, spot measurements were performed at all drip sites. The number of drips per minute were counted during each visit using a stopwatch and counting at least 10 drips. Second, continuous measurements were carried out at four drip sites WP 1-1, WP 1-2, WP 1-3, and WP-2 using acoustic Driptych Stalagmate drip loggers (http://www.driptych.com/).

3.4 Oxygen and hydrogen isotopes of water

The oxygen and hydrogen isotope composition ($\delta^{17}O$, $\delta^{18}O$ and δD) of dripwater and stream water was measured using cavity ring down spectroscopy (CRDS) (Steig et al., 2014). Dripwater samples collected between August 2016 and April 2017 were analysed for $\delta^{18}O$ and δD using a Picarro L1102-i water isotope analyzer at the Godwin Laboratory for Paleoclimate Research, University of Cambridge, UK. Samples collected between June 2017 and February 2018 were analysed for $\delta^{17}O$, $\delta^{18}O$ and δD using a Picarro L2140-i at the School of Environmental Sciences of the University of St. Andrews, UK. Samples collected from March 2018 to February 2019 were measured for $\delta^{17}O$, $\delta^{18}O$ and δD on a Picarro L2140-i at the Department of Biology and Geology at the Universidad de Almería, Spain. This instrument permits measurement of the triple oxygen and hydrogen isotope composition of liquid water with no sample pretreatment. The CRDS devices were interfaced with an A0211 high-precision vaporizer.

The results were normalized to the V-SMOW (Vienna-Standard Mean Ocean Water) scale by analyzing internal standards before and after a set of measurements of 10 to 12 samples. Three internal water standards (JRW, BOTTY and SPIT) were calibrated against V-SMOW and SLAP (Standard Light Antarctic Precipitation), using $\delta^{17}O$ values of 0.0 ‰ and -29.69865 ‰, respectively, and $\delta^{18}O$ values of 0.0 ‰ and -55.5 ‰, respectively (Schoenemann et al. 2013). This standardization considers $^{17}O_{excess} = 0$ for both international standards. δD was calibrated against V-SMOW, GISP (Green Ice Sheet Precipitation) and

SLAP. All isotopic deviations are reported in parts per thousand (‰) relative to V-SMOW. $^{17}O_{excess}$ values are given in per meg units (0.001 ‰), where $^{17}O_{excess} = \ln(\delta^{18}O/1000+1)-0.528*\ln(\delta^{17}O/1000+1)$ (Barkan and Luz, 2005). The $^{17}O_{excess}$ expresses a small $\delta^{17}O$ deviation (normally a few per meg units) of a water sample with respect to the Global Meteoric Water Line (GMWL) for triple oxygen isotopes, for which the slope is 0.528 (Luz and Barkan, 2010). The d-excess describes the deviation for $\delta^{18}O$ and δD of a given sample with respect to the GMWL ($\delta D-8*\delta^{18}O$; Craig et al., 1961).

The long-term precision (1σ) of oxygen and hydrogen isotope analyses was evaluated by measuring an internal standard (BOTTY) every 5-6 samples. The long-term precision on the Picarro L1102-i was ± 0.08 ‰ for $\delta^{18}O$ and ± 0.7 ‰ for δD (n = 33), while on the Picarro L2140-i it was ± 0.03 ‰, ± 0.05 ‰ and ± 0.4 ‰ for $\delta^{17}O$, $\delta^{18}O$, and δD, respectively (n = 43). The long-term precision for the d-excess parameter ($\delta D-8*\delta^{18}O$) was ± 0.7 ‰ on the Picarro L1102-i and ± 0.3 ‰ on the Picarro L2140-i. The long-term precision for $^{17}O_{excess}$ was ± 8 per meg. The calibrated value of BOTTY was indistinguishable within analytical errors when using the three different instruments, suggesting results are comparable.

3.5 Major and trace elements in dripwater

Elemental and major cation concentrations in cave stream, drip- and rainwater were measured on two generations of instruments at the University of Waikato. Samples collected between August 2016 and October 2017 were analysed using a Perkin Elmer Elan quadrupole ICP-MS, and samples collected between November 2017 and February 2019 were analysed with an Agilent 8900 triple quadrupole ICP-MS at the Waikato Environmental Geochemistry Laboratory. The precision of both instruments is similar and all relative standard deviations (RSDs) were <5%. The ICP-MS was optimized to maximum sensitivity daily, ensuring oxides and double-charged species were less than 2 %. External calibration standards were prepared using a IV71-A multi element standard from 0.1 to 500 ppb for trace elements and single element standards were used to prepare calibration standards for major elements Ca, Fe, Si, P, S, K, Na. An internal standard containing Sc, Ge, Te, Ir, and Rh was used for all samples. Check standards were analysed every 20 samples and re-calibration was performed every 100 samples. Blank samples were analysed every 10 samples to ensure minimal carryover between analyses.

3.6 Data analysis

In order to characterize the hydrological behavior of the drip sites the coefficient of variation (CV) (Smart and Friederich, 1987; Baldini et al., 2006) was calculated for discharge relative to the time of data collection (CV % = σ/ū x 100, with σ being the standard deviation, and ū the mean). Cross-correlation analysis between cumulative antecedent rainfall and drip rates was used to identify the response time of the drip sites to the rainfall amount during the monitoring period. Cluster analysis was employed to classify the drip sites according to hydrological similarities. Linear regressions were used to visualise the relationships between dripwater Mg/Ca and Sr/Ca ratios, the cave air CO_2 and cave air temperature as well as between rainfall amount and water isotopes. From these analyses a determination coefficient R^2 and *p* values were calculated. P values <0.05 were considered to be statistically significant.

4 Results

4.1 Local meteorology

The available daily precipitation and temperature datasets from the stations at Waipuna, Otorohanga Glenbrook, and Te Kuiti Ews show the same pattern when overlapped, although the amplitudes differ (Figure 3). The Waipuna meteorological station records large variations in annual surface temperature, with minimum and maximum temperatures ranging from -0.6°C in July to 33°C in January. Daily precipitation ranged from 118 mm in May 2017 to 51 mm in December 2018, without any

pronounced seasonality. The driest months are typically November and December (austral summer), and the wettest months are August and September. While the variability and timing of rainfall at the three stations have the same seasonal structure, the Waipuna rain station typically recorded higher amounts. This is consistent with its higher altitude (~90 m) relative to Otorohanga Glenbrook (40 m) and Te Kuiti Ews (62 m), and thus indicates an orographic effect on rainfall.

The mean monthly surface conditions (2002–2019) from Te Kuiti Ews station are shown in figure 4. These comprise monthly mean rainfall, monthly mean temperature, potential evapotranspiration (PET), and effective rainfall (P_{eff}), calculated as the difference between P and PET.

4.2 Waipuna Cave hydrology

All drip sites were hydrologically active during the monitoring period, with variable mean discharges between 10.5 and 22.1 μL s^{-1}. The CV of the drip sites varied between 31 and 149 % (Table 1). Cross-correlation analysis between antecedent cumulative rainfall and drip rate time series from the acoustic drip loggers show different lag times for each drip. These are 19 days for WP 1-1, 15 days for WP 1-2, 16 days for WP 1-3, and 4 days for drip point WP-2 (Table 1, Fig. 5). For the drip sites where drip rates were only measured manually during the cave visits, the observed lags were 18 days for WP 1-4 and WP 1A, 11 days for WP 1B and WP-3, and 6 days for WP-4. Cluster analysis using manual and logger data reveals three main groups of drip sites based on 25 observations of discharge at each drip site with 4 common data points among them (Fig. 6). Based on the cluster analysis we identified three flow types, defined hereafter as Type 1, which includes drip sites with the slowest response to rainfall (WP 1-1, WP 1-2, WP 1-4 and WP-4); Type 2, which isolates drip WP-2 with the fastest response to rainfall; and Type 3, which includes drip sites WP 1-3 and WP-3 with intermediate response time to rainfall. For comparison we have also located the drip sites in the classification grid of Smart and Friederich (1987) (Supplement figure S1), which will be discussed in section 5.1.

4.3 Isotope geochemistry

Dripwater oxygen isotope values varied between -3.0 and -2.4 ‰ for $\delta^{17}O$, -5.8 and -5.2 ‰ for $\delta^{18}O$, and -32.7 and -28.3 ‰ for δD. The d-excess ranged from 8.8 to 15.4 ‰ (Supplement S5). All dripwater $\delta^{18}O$ and δD values fall on the local meteoric water line (LMWL, $\delta D = 7.15*\delta^{18}O+7.6$) as determined from rainwater samples from the Waikato region in the North Island (Fig. 7) (Keller, 2014). A linear regression of all dripwaters is expressed as $\delta D = 5.05*\delta^{18}O-2.3$. The very low intercept of -2.3 is the result of the very narrow range of the dripwater cluster and is not related to secondary evaporation. The $\delta^{18}O$ values of the cave stream are in the same range as the dripwaters, but δD values are ~ 20 ‰ higher ($\delta D = 5.9*\delta^{18}O+3.4$). The d-excess of the stream water ranged from 9.4 to 15 ‰.

All dripwater $\delta^{17}O$ and $\delta^{18}O$ values fall close to the GMWL (Supplemental fig. S2), the equation for which is $\ln(\delta^{17}O/1000+1) = 0.528 \ln(\delta^{18}O/1000+1) +0.00033$ (Luz and Barkan, 2010). The mean $\delta^{17}O$ deviation with respect to the GMWL ($^{17}O_{excess}$) in the dripwater is 26±8 per meg, with the values ranging from 6 to 44 per meg. The $^{17}O_{excess}$ values of the cave stream were 25±4 per meg on average.

Between September 2016 and June 2017, drip sites WP 1-1, WP 1-2, WP 1-3, WP 1-4, WP 1A, and WP 1B showed low variability in dripwater $\delta^{18}O$ and δD, with ranges of 0.5 ‰ (-5.4 to -5.9 ‰) in $\delta^{18}O$ and 3.9 ‰ (-28.8 to -32.7 ‰) in δD, and mean values of -5.61±0.04 ‰ (2σ) and -31.01±0.4 ‰, respectively. Although small, this range is still greater than the analytical error of 0.16 ‰ and 1.4 ‰, respectively (Figs. 8b, c and S3). From July 2017 to January 2019 virtually no variability was observed in $\delta^{18}O$ and δD (Figs. 8b, c and S3). The dripwater $\delta^{18}O$ and δD in that period have ranges 0.3 ‰ (-5.4 to -5.7 ‰) in

$\delta^{18}O$, and 2.16 ‰ (-29.2 to -31.3 ‰) in δD, with mean values of -5.61±0.05 ‰ (2σ) and -30.47±0.18 ‰. This range is virtually at the analytical uncertainty level.

By contrast, the three drip sites with the shortest lags, WP-2, WP-3, and WP-4, exhibit higher variability in $\delta^{18}O$ and δD. In particular, sites WP-2 and WP-3 show a marked increase (0.5 ‰) in $\delta^{18}O$ between December 2016 and January 2017 (Fig. 8a). $\delta^{17}O$ varies in the same way as $\delta^{18}O$ (Supplement S4).

4.4 Dripwater major and trace elements

Here we report elemental composition data for those components typically influenced by PCP, i.e. Ca concentration (Fairchild et al., 2000) and Mg/Ca and Sr/Ca ratios (Tremaine et al., 2016). Dripwater Ca concentrations range from 0.7 to 2.2 mol L^{-1}, Mg/Ca varied from 17.7 to 66.5 and Sr/Ca varied from 0.24 to 1.11 (mmol mol^{-1}). All drip sites show a strong positive correlation between Mg/Ca and Sr/Ca ratios, with coefficients of determination varying from 0.68 to 0.9 (Fig. 10b). The two different trends observed in the relationship between Mg/Ca and Sr/Ca ratios will be discussed in section 5.5. The temporal variability of the Mg/Ca and Sr/Ca ratios shows three noticeable peaks for all drip sites during the summers of 2017 (February), 2018 (January) and 2019 after the previously reduced effective rainfall. Dripwaters collected during late summer (January-February) generally had higher Mg/Ca and Sr/Ca ratios and lower Ca concentrations, while samples collected in winter (July-August) had the lowest Mg/Ca and Sr/Ca ratios and the highest Ca concentrations (Fig. 11 and Supplement S6).

4.5 Cave air temperature and CO_2

Daily cave air temperature in the Organ Loft chamber recorded between June 2017 and May 2018 varied between 7.4°C and 11.7°C (mean 10.4°C) (Fig. 12a, b), with the highest temperatures measured in summer (February and March) and the lowest temperatures in winter (July and August). The air temperature logger at Waipuna Cave meteorological station recorded temperatures between -0.6°C and 29.3°C. The temperature difference (ΔT) between Waipuna Cave air and the external air shows an annual cycle (Fig. 12c), ranging from -22°C to 8.3°C, with a mean of -2.1°C. The largest negative ΔT values occurred from late spring November 2017 to early autumn April 2017 owing to the marked increase in external temperature.

Cave air pCO_2 varied from a minimum of 438 ppm in September 2016 to a maximum of 930 ppm recorded in March 2019 (Fig. 12b). Cave air pCO_2 is positively correlated with cave air temperature ($R^2 = 0.67$, $p = 0.045$). The highest air pCO_2 values are registered when cave air temperature reaches its maximum in summer and decrease when cave air temperature is lowest in winter (see the discussion in Section 5.4).

5 Discussion

This work aims to evaluate the hydrochemical response of Waipuna Cave to environmental dynamics, and to test its suitability for speleothem-based palaeoclimate reconstructions. We explore the links between the physiochemical parameters measured in Waipuna Cave and rainfall and temperature changes at seasonal to inter-annual timescales. Our results show that Waipuna Cave reflects the external environmental dynamics on inter-annual timescales. The results and interpretation of monitoring data constitute a solid platform for the interpretation of speleothem-based reconstructions that are currently under construction.

5.1 Waipuna Cave hydrology

The meteorological data from Otorohanga Glenbrook and Te Kuiti Ews stations are considered suitable for evaluating the Waipuna Cave monitoring data, given the rainfall patterns are similar to those at Waipuna. The monitored drip sites in Waipuna

Cave are highly sensitive to rainfall variability, demonstrating the free draining nature of the overlying soil and the relatively thin bedrock overburden.

Our results indicate that the monitored drip sites respond to three different infiltration pathways: i) Type 1 via diffuse, ii) Type 2 via fracture, and iii) Type 3 via combined flow. Type 1 drips WP1-1, WP 1-2, WP 1-4, and WP 1A show the slowest response to rainfall (lagging between 11 and 19 days). These drips belong to the Organ Loft curtain, which strongly supports the hypothesis that these sites are hydrologically connected to each other. Given that the curtain is part of the continuum from the ceiling to the floor (ca. 6 m height), it is likely that all its drip sites are mainly fed via diffuse flow through the limestone matrix, which is a function of the primary porosity of the karst (Bradley et al., 2010). Type 2 is represented by drip sites WP-2 and WP-4, which are located in the upper gallery of the Organ Loft at a greater ceiling height. These drips have a faster response (4 to 6 days) to antecedent rainfall, suggesting that these drips are controlled mainly by fracture flow. This is consistent with the clear identification of zones of structural weakness along the ceiling (physically representing fault or joint-like structures) and the shorter vadose flow path at these locations. The cross-correlation of the antecedent rainfall and the drip rates agrees with the cluster output for all drip sites except drip site WP-4, which has a response time of 4 days but clusters with the group of drip sites with a lag of 18 to 24 days. This can be explained by the limited size of the dataset: the drip rates of WP-4 were measured only manually, thus limiting the input for the cluster analysis compared to drip sites monitored with loggers. Finally, we grouped WP 1-3 and WP-3 into flow type 3, because these two drip sites have similar intermediate response rates to rainfall (11 days), independent of their location in the Organ Loft chamber which is in the ceiling of the upper gallery for WP-3 and the flowstone curtain for WP 1-3. It is likely that these drips are fed by a combination of fracture and matrix flow (Mahmud et al., 2018).

Although the response time varies from days to 2–3 weeks, all drip sites forming stalagmites and feeding the flowstone reflect precipitation dynamics at sub-annual scale. The three types of drip discharge in Waipuna Cave do not satisfactorily fit into the classification model of Smart and Friederich (1987) which locates drip sites WP 1A, WP 1B and WP-3 fall in the seepage flow and sites WP 1-1, WP 1-2, WP 1-3, WP 1-4, WP FB, WP-4, and WP-2 in the fracture flow range (Supplement figure S1).

5.2 Rainwater isotope geochemistry

The distribution of the rainwater oxygen and hydrogen isotopes along the LMWL (Fig. 7) does not reveal a clear seasonal pattern. However, when comparing rainfall $\delta^{18}O$ values with the amount of precipitation across the entire monitoring period (Fig. 13, black line), we observe a positive relationship ($R^2 = 0.56$, $p = <0.0001$). The strongest correlations between rainfall amount and $\delta^{18}O$ values are observed in austral spring and summer ($R^2 = 0.68$ $p = 0.0002$, and $R^2 = 0.89$ $p = 0.0001$, respectively) when temperature is highest in the Waikato area (Fig. 13, green and orange lines). Among the various climatic and geographical effects on the isotopic composition of rainwater, the 'amount effect' has been shown to significantly influence rainwater $\delta^{18}O$ in sub-tropical regions. The amount effect is the empirical negative correlation between rainfall amount and rainwater $\delta^{18}O$ (Dansgaard 1964) which arises from the partial re-evaporation and thus isotopic enrichment of rain droplets falling through relatively dry air below cloud level during periods of reduced precipitation (Dansgaard, 1964; Risi et al., 2008; Lachniet 2009; Breitenbach et al. 2010). This process affects the isotopic signature in rainfall observed in the Waitomo region in spring and summer, but not during the winter season when re-evaporation from falling rain is minimal due to high relative humidity. (this is reflected in lower R^2-values samples from April to September, Fig. 13). In the wet season rain droplets are less affected by re-evaporation and remain unaltered with respect to $\delta^{18}O$. These observations suggest that regional atmospheric conditions, associated with ENSO dynamics or strength of the Westerlies, can impose their signature on the isotopic composition of precipitation.

Dripwater $\delta^{18}O$ and δD values closely reflect the mean isotopic composition of the rainwater (Fig. 7). The isotope signatures of dripwaters from the Organ Loft curtain lack seasonal patterns as they are decoupled from recharge rates by a significant epikarst store (Fig. 8b, c and S3c). Instead, homogenization in the epikarst reservoir controls the isotopic composition of the water feeding the Organ Loft curtain. As highlighted in Figure 7, $\delta^{18}O$ values vary minimally around a mean dripwater $\delta^{18}O$ value of -5.6 ‰, which is only slightly lower than the average rainwater value (-5.15 ‰, Keller 2014). This similarity indicates rapid mixing of freshly infiltrating water with older water in the epikarst, as also found in earlier studies from the Waitomo district (Williams and Fowler, 2002) and elsewhere (Mattey et al., 2008; Tremaine et al., 2016; Breitenbach et al., 2019). The observed buffering of dripwater towards the mean rainwater $\delta^{18}O$ value suggests that speleothem $\delta^{18}O$ ratios can be expected to reflect multi-annual to multi-decadal changes in rainfall isotope geochemical patterns. Furthermore, it may be possible that speleothems from Waipuna Cave record a long-term temperature signal that is un-biased with regard to seasonal infiltration changes. On the other hand, this pattern might also indicate that Waipuna Cave speleothem isotope geochemistry is insensitive to sub-seasonal changes in rainfall $\delta^{18}O$ and δD ratios. Flowstone $\delta^{18}O$ values originating from water from these drips are unlikely to reflect atmospheric dynamics related to seasonal or ENSO variability, and other proxies must be used instead to identify these dynamics.

Waipuna Cave dripwaters do not show significant variations in $^{17}O_{excess}$ over time and most results overlap within analytical errors (Fig. 9). Recent investigations into triple oxygen isotopes in mid-latitude rainfall have reported seasonal oscillations in $^{17}O_{excess}$ that have been attributed to changes in relative humidity at the moisture source (i.e., where the water vapour originates), or to swings between different moisture sources with evaporation occurring under different environmental conditions (Affolter et al., 2015; Uechi and Uemura, 2019). Unlike d-excess, $^{17}O_{excess}$ in rainfall is apparently almost exclusively controlled by relative humidity at the water-vapour boundary layer (i.e. the interface between water and free atmosphere), with insignificant temperature effects (Luz and Barkan, 2010). Thus, if there are seasonal changes in the dominant moisture source and origin of storms for the Waikato area, these would be likely to affect local precipitation and this variability could be recorded in Waipuna Cave dripwater. However, no significant variations in $^{17}O_{excess}$ are found over the studied period (September 2017 to October 2018), suggesting that the isotope values of meteoric water are homogenized in the epikarst, and that Waipuna Cave dripwater $^{17}O_{excess}$ is insensitive to (sub-) seasonal changes. We suspect that, as with $\delta^{18}O$ ratios, the interannual response of cave dripwater might be controlled by long-term variations in the $^{17}O_{excess}$ of rainfall and changes in the relative importance of ENSO and the southern Westerlies. However, given the narrow range of $^{17}O_{excess}$ in rainwater in the mid-latitudes (normally < 30 per meg, Luz and Barkan, 2010) and the relatively large errors of current analytical methods (i.e., ~ 8 per meg), longer (i.e. multi-decadal) dripwater monitoring would be needed to test this hypothesis.

The fracture-flow fed drip sites WP-2, WP-3, and WP-4 are more sensitive to variations in surface conditions and were likely affected by a moderate drought in the summer of 2016-2017 (Fig. 8a). 2016 was the warmest year on record for New Zealand, with average annual temperatures 0.5 to 1.2°C above normal (NIWA annual climate summary 2016). Rainfall was 50-79 % below average in December 2016, causing anomalously low soil moisture levels (NIWA summer 2016-17 report). Hence the January 2017 $\delta^{18}O$ values of -5.08 and -5.12 ‰ (Fig. 8a) might have been affected by the reduced infiltration caused by the higher evapotranspiration relative to precipitation.

The rapid decrease in dripwater $\delta^{18}O$ at the fast drip sites in March and April 2017 could have been caused by aquifer recharge (Fig. 8a). The decrease coincides with a period of increased precipitation, which would have quickly infiltrate the relatively dry soil and entered the aquifer. This is consistent with the short water residence time of 5 days, and the greater degree of fracture flow and vadose zone influence at these sites compares with the slower drip sites.

5.3 Dripwater major and trace elements

Detecting short-term (sub-seasonal to annual) hydrological changes related to environmental conditions above Waipuna Cave requires sensitive (and ideally quantitative) proxies. In the following, we review the parameters we have measured in terms of their sensitivity.

Negative effective precipitation (P_{eff}), either from reduced rainfall or enhanced PET, can enhance degassing of CO_2 from the epikarst zone, and thus prior calcite precipitation (PCP) in the epikarst (Fairchild et al., 2000). Another factor potentially controlling PCP is cave ventilation. Enhanced ventilation removes moisture and CO_2 from the cave environment, which can result in < 100 % relative humidity (RH) and/or near-atmospheric CO_2 concentrations in cave air (Gázquez et al., 2016). Low cave air RH values can lead to dripwater evaporation, while low cave air pCO_2 can enhance dripwater degassing and formation of speleothems at the cave ceiling. Both processes can affect X/Ca and stable isotope ratios (Fairchild et al., 2006a; Breitenbach et al., 2015). Normally, the processes in the epikarst and in the cave act in concert and cannot be disentangled. Here, we show that detailed monitoring of X/Ca dynamics in drip water can give valuable insights into the relative importance of these two zones, namely the epikarst and cave itself, for PCP intensity.

The PCP predictor line represents the modeled evolution of the Ca_{aq} concentration which precipitates calcite in equilibrium as pCO_2 decreases from the soil to the cave (Fairchild et al., 2006b). The Mg/Ca ratios of Waipuna Cave dripwaters closely follow the PCP predictor line (Fig.10a). Mg/Ca and Sr/Ca ratios are plotted in Fig. 10b and a strong positive correlation is observed in Waipuna Cave dripwaters ($R^2 = 0.82$, $p = <0.001$) (Sinclair et al., 2012; Tremaine and Froelich, 2013). This effect has also been widely identified in cave systems in Australia, with a climate similar to the Waitomo region. For example, Harrie Wood Cave dripwater Mg/Ca and Sr/Ca ratios show enhanced PCP during dry periods associated with El Niño, and reduced PCP during La Niña events (Tadros et al. 2016).

The degree of PCP could be expected to be linked to infiltration rates, with fracture flow being prone to more PCP because it empties faster compared to seepage flow. As long as the epikarst remains water-filled, PCP would be minimized, whereas fast drying of the epikarst results in intrusion of soil air which might induce PCP. The fracture flow-fed drips can be distinguished from seepage flow-fed ones by lower Ca concentrations and increased scatter around the predicted PCP line (Fig. 10a). This can be explained by somewhat shorter interaction between the infiltrating water and the host rock. When comparing the elemental composition of the different drip sites (Fig. 10b), we observe that all drips show comparable Mg/Ca and Sr/Ca ratios, suggesting that all drips are similarly affected by PCP. The different infiltration lag time of the individual drips thus does not appear to affect the extent of PCP in Waipuna Cave.

Although rainfall is evenly distributed throughout the year, a strong seasonal PCP signal is found in the dripwater for all drip sites across the whole monitoring period (Fig. 11). Lower Mg/Ca and Sr/Ca ratios occurred in the wettest months, when precipitation exceeded evapotranspiration. Conversely, higher Mg/Ca and Sr/Ca ratios are found in the driest months (i.e. November to March) when the potential evapotranspiration exceeds rainfall and effective infiltration is negative (Fig. 11 and Supplement S6). Hydrological changes thus govern epikarst PCP, which in turn controls dripwater Mg/Ca and Sr/Ca ratios (Fig. 10b). This observation supports our hypothesis that Waipuna Cave dripwaters are capable of registering changes in local hydrology, with seasonal differences being most strongly expressed in Sr/Ca ratios. Changes in Sr/Ca ratio potentially reflect the interplay of PCP and enhanced selective Sr leaching (incongruent dissolution), which both operate to increase Sr/Ca in the drier months (Sinclair et al., 2012), while the wetter months are characterised by infiltration and reduced selective Sr leaching (congruent dissolution) (see Section 5.5).

5.4 Cave ventilation

Monitoring of temperature and CO_2 between June 2017 and June 2018 shows that Waipuna Cave ventilation is driven by changes in the density of internal and external air in response to seasonal external temperature (Fig. 12), i.e., Waipuna Cave is a barometric cave *sensu* Fernandez-Cortés et al. (2008). This behavior has been observed in other caves globally.

During late spring and summer (November 2017 to May 2018), cave air is colder than surface air ($\Delta T < 0$) (Fig. 12c). A greater relative density of the cave air and the pressure difference compared to the surface air creates a cold air 'lake' within the cave. This cold air mass is isolated from the warmer, less dense, exterior air (i.e., isolation period) due to the geometry of the cave (Fig. 14). The cold, stagnant cave air inhibits exhalation of CO_2 released from the dripwater, which then accumulates in the cave atmosphere. Inversely, from autumn to early spring (June 2017 to October 2017), a positive ΔT (i.e. warmer cave air relative to the surface, though still colder than summer cave air) leads to barometric ventilation of cave air (Fig. 12c). Due to the pressure gradient, cool and dense surface air will sink into the cave, whilst rising warm cave air leaves the cave. The intensified air exchange promotes CO_2 extraction from the cave. This effect is reflected in the positive relation between $T_{cave\ air}$ and CO_2 values ($R^2 = 0.67$, $p = 0.04$). These two phases of cave ventilation dynamics fit the chimney circulation model (Fairchild and Baker, 2012) and have been observed in similar climatic settings in the USA (Oster et al., 2012), India (Breitenbach et al., 2015) and Spain (Gazquez et al., 2017) among others.

Furthermore, we find that during the period with negative P_{eff}, normally the summer season, the relationship between Mg/Ca and Sr/Ca ratios is more pronounced, reflected in a higher R^2 value ($R^2 = 0.92$, $p < 0.001$) and a steeper slope compared to the winter season ($R^2 = 0.52$, $p < 0.001$), when this relationship is less strong, and the slope is lower (Supplement S7). Together with lower dripwater X/Ca values in the winter season, this suggests a less significant role for PCP at times of higher ventilation and CO_2 changes in Waipuna Cave. Since all Mg/Ca and Sr/Ca ratios fall along the PCP line during the months of reduced ventilation (November–March), it seems that enhanced cave ventilation does not affect PCP.

5.5 The ENSO signature in Waipuna Cave

We have demonstrated that in Waipuna Cave, Mg/Ca and Sr/Ca ratios are sensitive PCP indicators. Here we discuss how they potentially react to infiltration changes governed by ENSO dynamics.

A plot of Mg/Ca versus Sr/Ca ratios displays two clusters, each along a clear trend (Figs. 9b and 14). Orange data points indicate all samples collected between October 2016 and February 2019, minus the period that comprises the blue group of samples. Blue-coloured symbols represent samples collected between February 2018 and the end of August 2018, a period with above-average rainfall, likely related to a La Niña event that developed in December 2017. These conditions prevailed over the following months (January to March 2018) (NIWA 2018a). Even though La Niña dissipated in March 2018, it still affected early autumn circulation patterns in the central North Island, expressed generally by stronger than usual northeasterly winds, average temperatures 1.2°C higher than normal, well above normal rainfall (> 149 % of normal), and much higher soil moisture levels for this time of year (NIWA, 2018b). Dripwater samples collected before February 2018 and after August 2018 (ENSO-neutral conditions), plot on the main PCP trend, but samples collected between February 2018 and August 2018 (during La Niña event decay) plot on a distinct line (Fig. 15). Some water samples collected on 7th February 2018 fall into the same range as the orange (stronger PCP) group, while others collected on the same day, fall into the range of the blue group, supporting our notion that the cave's hydrology reacts within days to weeks (depending on drip lag response) to infiltration changes.

It therefore seems possible to identify ENSO events by singling out different regression trends in Sr/Ca-Mg/Ca space (Fig. 15). Our data, combined with meteorological information, suggest different behavior of Sr/Ca during the warm/wet La Niña

event. A comparison of intercept values of the two trendlines suggests that wet La Niña conditions promoted higher effective infiltration, thereby reducing Sr availability.

Mg/Ca and Sr/Ca ratios are lower during winter, the wettest months with the lowest PET. Conversely, Sr/Ca and Mg/Ca ratios are higher in the higher PET, drier summer months (Fig. 11 and Supplement S7). We postulate that in Waipuna Cave, the La Niña climate mode, although short-lived, has a strong influence on Sr/Ca variation that produces an overprint on PCP dynamics. In the case of the 2017 La Niña event, we interpret the data to indicate that the extra infiltration associated with the event fundamentally altered the regime of host rock dissolution, thereby decreasing Sr availability (Fairchild and Treble 2009) in a manner consistent with congruent host rock dissolution and reduced selectivity in Sr leaching (Fairchild et al., 2000). In summary, we argue that hydrological change associated with ENSO, which amplifies the length of the 'wet' time window, should modulate Sr/Ca to a greater extent than seasonal changes.

6 Conclusions

The results of a three-year long multi-parameter monitoring campaign in Waipuna Cave help to characterise the sensitivity of the cave with respect to external climatic changes occurring on intra- and interannual time scales in the North Island of New Zealand. The monitored parameters include drip rates, cave air temperature, dripwater trace elements, water stable isotopes, and cave air pCO_2. These were compared to meteorological data from nearby stations. Based on geochemical and drip rate data, we identify three distinct infiltration pathways for the studied drip sites. These are Type 1: diffuse flow, Type 2: fracture flow, and Type 3: combined flow, with lagged responses to antecedent rainfall of 24–18 days, 4–6 days, and 11 days, respectively. Waipuna Cave thus reacts quickly (within less than one month) to external precipitation variability and is sensitive to sub-seasonal changes in epikarst hydrology.

Dripwater isotope composition in Waipuna Cave reflects the mean rainwater $\delta^{17}O$, $\delta^{18}O$, and δD values. Mixing processes in soil and epikarst obscure any seasonal isotopic signal in the dripwater. However, long-term (i.e., inter-annual to decadal) atmospheric changes are very likely recorded by speleothem calcite $\delta^{18}O$ and $^{17}O_{excess}$ in Waipuna Cave. Because local spring and summer rainfall isotope values are influenced by the amount effect, pronounced droughts can affect the isotopic composition of the dripwater, and that signal may be recorded in speleothems.

Dripwater Mg/Ca and Sr/Ca ratios are modulated by PCP and reflect local hydrological changes. Higher Mg/Ca and Sr/Ca ratios reflect periods of reduced effective infiltration from November to March when the potential evapotranspiration exceeds local rainfall amount. The relationship between Mg/Ca and Sr/Ca ratios may be affected by ENSO variability, with wetter conditions and reduced PCP occurring during La Niña events reflected in lower Mg/Ca-Sr/Ca slopes. This relationship may thus be a sensitive geochemical tracer of ENSO dynamics. However, longer monitoring is required to validate this interpretation.

Surface air temperature changes govern cave ventilation in Waipuna Cave. Enhanced ventilation occurs between April and October (austral winter) when the surface air temperature is lower than in the cave. During austral summer surface air temperatures are higher than cave air temperatures, resulting in reduced ventilation by virtue of a cold cave air lake. The Waipuna Cave ventilation pattern is an important factor controlling dripwater degassing, cave air CO_2 dynamics, speleothem growth rates, and isotope fractionation.

The findings of this study on the hydrochemistry in Waipuna Cave establish a baseline that will allow interpretation of speleothem-based proxy records at seasonal and interannual scales to reconstruct local hydrological changes as well as regional dynamics e.g. ENSO events. Longer-term monitoring is required in order to better constrain the effects of synoptic-scale environmental fluctuations on speleothem records from Waipuna Cave and nearby caves.

Data and samples availability

Data reported here will be made fully available to the public via a public domain platform. Additionally, data can be requested from the corresponding author (CN, cinthya.navafernandez@rub.de).

Author contributions

CN conducted fieldwork, collected the samples and data, analysed the data, and prepared the original manuscript. AH designed and carried out the cave monitoring programme, conducted fieldwork, and supervised the study. FG conducted the stable water analyses and contributed to the discussion of the results. OK participated in the fieldwork, contributed to the discussion, helped with figures, supervised the study, and contributed to the discussion. NM helped with statistical analysis and discussion. BF conducted fieldwork and helped with the statistical analysis and writing. JH contributed with fieldwork and structure from motion images. AP and BW helped in the cave monitoring effort. AF carried out the major and trace elements analysis and contributed to the discussion. DH provided laboratory resources and helped in the acquisition of funding. AI contributed with the editing process. SB designed the monitoring programme, supervised the study, collected samples, and contributed to the interpretation, visualization, and preparation of the manuscript.

Competing interests

The authors declare that they have no conflict of interest.

Acknowledgments

Thanks to Ingrid Lindeman, Inken Heidke, Jackson White for their valuable fieldwork contributions. We thank Peter and Libby Chandler for their permission to access Waipuna Cave and their ongoing support of research. C.N.F. acknowledges financial support from the German Academic Exchange Service (DAAD). F.G. was financially supported by the "HIPATIA" research program of the University of Almería. This study received funding from the European Union's Horizon 2020 Research and Innovation programme under the Marie Skłodowska-Curie grant agreement No 691037 and Royal Society of New Zealand grant agreement RIS-UOW1501, and Rutherford Discovery Fellowship (RDF-UOW1601) to A.H.

References

Affolter S., Häuselmann, A.D., Fleitmann, D., Häuselmann, P., and Leuenberger, M., Triple isotope (δD, $\delta^{17}O$, $\delta^{18}O$) study on precipitation, drip water and speleothem fluid inclusions for a Western Central European cave (NW Switzerland), Quaternary Sci. Rev., 127, 73–89, doi.org/10.1016/j.quascirev.2015.08.030, 2015.

Asmerom, Y., Polyak, V. J., and Burns, S. J.: Variable winter moisture in the southern United States linked to rapid glacial climatic shifts, Nat. Geosci., 3, 114–117, doi.org/10.1038/ngeo754, 2010.

Baldini, J. U. L., McDermott, F., and Fairchild, I. J.: Spatial variability in cave drip water hydrochemistry: Implications for stalagmite paleoclimate records, Chem. Geol., 235,390–404, doi.org//10.1016/j.chemgeo.2006.08.005, 2006.

Baker, A., Barnes, W. L. and Smart, P. L.: Variations in the discharge and organic matter content of stalagmite drip waters in Lower Cave, Bristol, Hydrol. Process., 11, 1541–1555, doi.org/10.1002/(sici)1099-1085(199709)11:11<1541::aid-hyp484>3.0.co;2-z, 1997.

Barkan, E. and Luz, B.; High precision measurements of $^{17}O/^{16}O$ and $^{18}O/^{16}O$ ratios in H_2O, Rapid Commun. Mass Sp. 19, 3737–3742, doi.org/10.1002/rcm.2250, 2005.

Basher, R.E.: The 1997/98 El Niño Event: Impacts, responses and outlook for New Zealand, Ministry of Research, Science and Technology, Wellington. Report No. 73. 28 p., 1998.

Bradley, C., Baker, A., Jex, C. N., and Leng, M. J.: Hydrological uncertainties in the modelling of cave drip-water $\delta^{18}O$ and the implications for stalagmite palaeoclimate reconstructions, Quaternary Sci. Rev., 29, 2201–2214, doi: 10.1016/j.quascirev.2010.05.017, 2010.

Breitenbach, S.F.M., Adkins, J. F., Meyer, H., Marwan, N., Kumar, K.K., and Haug, G. H.: Strong influence of water vapor source dynamics on stable isotopes in precipitation observed in Southern Meghalaya, NE India, Earth. Planet. Sc. Lett., 292, 212–220, doi.org/10.1016/j.epsl.2010.01.038, 2010.

Breitenbach, S.F.M., Lechleitner, F.A., Meyer, H., Diengdoh, G., Mattey, D., and Marwan, N.: Cave ventilation and rainfall signals in dripwater in a monsoonal setting- a monitoring study from NE India. Chem. Geol., 402,111–124, doi.org/10.1016/j.chemgeo.2015.03.011, 2015.

Breitenbach, S.F.M., Plessen, B., Waltgenbach, S., Tjallingii, R., Leonhardt, J., Jochum, K. P., Meyer, H., Goswami, B., Marwan, N., and Scholz, D.: Holocene interaction of maritime and continental climate in Central Europe: New speleothem evidence from Central Germany, Global Planet. Change, 176, 144–161, doi.org/10.1016/j.gloplacha.2019.03.007, 2019.

Chen, S., Hoffman, S.S., Lund, D. C., Cobb, K.M., Emile-Geay, J., and Adkins J.F.: A high-resolution speleothem record of western equatorial Pacific rainfall: Implications for Holocene ENSO evolution, Earth Planet. Sc. Lett., 442, 61–71, doi.org/10.1016/j.epsl.2016.02.050, 2016.

Cheng H., Spötl C., Breitenbach, S. F. M., Sinha, A., Wassenburg, J. A., Jochum, P. K., Scholz, D., Li, X., Yi, Liang, Peng, Y., Lv, Y., Zhang, P., Votintseva A., Loginov, V., Ning, Y., Kathayat, G., and Edwards, L.: Climate variations of Central Asia on orbital to millennial timescales, Sci. Rep 6, 36975, http://doi.org/10.1038/srep36975, 2016.

Dansgaard, W.: Stable isotopes in precipitation, Tellus, 16, 436–468, 1964.

Dorale, J. A., Edwards, R. L., Ito, E., and Gonzalez, L.A.: Climate and vegetation history of the midcontinent from 75 to 25 ka: a speleothem record from Crevice, Science, 282,1871–1874, doi:10.1126/science.282.5395.1871, 1998.

Fairchild, I. J. and Baker, A.: Speleothem Science: From Process to Past Environments, Wiley-Blackwell, UK, 450, 2012.

Fairchild, I. J., Borsato, A., Tooth, A. F., Frisia, S., Hawkesworth, C. J., Huang, Y., McDermott, F., and Spiro, B.: Controls on trace element (Sr-Mg) compositions of carbonate cave water: implications for speleothem climatic records, Chem. Geol., 166, 255–269, doi.org/10.1016/S00009-2541(99)00216-8, 2000.

Fairchild, I. J., Smith, C. L., Baker, A., Fuller, L., Spötl, C., Mattey, D., and McDermott, F.: Modification and preservation of environmental signals in speleothems, Earth Sci. Rev., 75, 105–153, doi.org/10.1016/j.earscirev.2005.08.003, 2006a.

Fairchild, I. J. Tuckwell, G. W., Baker, A., and Tooth, A. F.: Modelling of dripwater hydrology and hydrogeochemistry in a weakly karstified aquifer (Bath, UK): Implications for climate change studies. J. Hydrol. 321, 213–231, doi: 10.1016/j.jhydrol.2005.08.002, 2006b.

Fernandez-Cortes, A., Calaforra, A., and Sanchez-Martos, F.: Hydrogeochemical processes as environmental indicators in drip water: study of the Cueva del Agua (Southern Spain), Int. J. Speleol. 37, 41–52, http://dx.doi.org/10.5038/1827-806X.37.1.4, 2008.

Ford, D., and Williams, P., Karst Hydrogeology and Geomorphology. John Wiley, Chichester, UK, 2007.

Frappier, A., Sahagian, D., Gonzalez, L.A., and Carpenter, S.J.: El Niño Events Recorded by Stalagmite Carbon Isotopes, Science, 298, 565, doi:10.1126/science.1076446, 2002.

Garr, C. E., and Fitzharris, B.B.: A Climate Classification of New Zealand based on Numerical Techniques, New Zealand Geographer, 47, 60–71, 1991.

Gazquez, F., Quindos-Poncela, L., Sainz-Fernandez, C., Fernandez-Villar, A., Fuente-Merino, I., and Celaya-Gonzalez, S.: Spatiotemporal distribution of $\delta^{13}C$-CO_2 in a shallow cave and its potential use as indicator of anthropic pressure. J. of Environ. Manage. 421–432, 180, doi.org/10.1016/j.jenvman.2016.05.078, 2016.

Gázquez, F., Calaforra, J. M., Evans, N. P., and Hodell D. A.: Using stable isotopes ($\delta^{17}O$, $\delta^{18}O$ and δD) of gypsum hydration water to ascertain the role of water condensation in the formation of subaerial gypsum speleothems. Chem. Geol. 452, 34–46, doi.org/10.1016/j.chemgeo.2017.01.021, 2017b.

Griffiths, G.M.: Changes in New Zealand daily rainfall extremes 1930-2004, Weather and Climate, 27, 3–44, doi.org/10.2307/26169689, 2006.

Griffiths, M. L., Kimbrough, A.K., Gagan, M. K., Drysdale, R. N., Cole, J.E., Kathleen, J.R., Zhao, J.-X., Cook, B.I., Hellstrom, J.C., and Hantoro, W. S.: Western Pacific hydroclimate linked to global climate variability over the past two millennia, Nat. Commun. 7, 11719, doi:10.1038/ncomms11719, 2016.

Hartland, A., Andersen, M.S., and Hamilton, D. P.: Phosphorus and arsenic distributions in a seasonality stratified, iron- and manganese-rich lake: microbiological and geochemical controls, Environ. Chem., 12, 708-722, https://doi.org/10.1071/EN14094, 2015.

Hartland, A., and Zitoun, R.: Transition metal availability to speleothems controlled by organic bindings ligands, Geochem. Perspect., 8, 22–25, doi:10.7185/geochemlet.1824, 2018.

Henderson, G.H.: Caving in to new chronologies, Science, 313, 620–622, doi:10.1126/science.1128980, 2006.

Hewitt, A. E.: New Zealand soil classification, Landcare Research Science Series, New Zealand ,1, 136, 2010.

Immenhauser, A., Buhl, D., Richter, D., Niedermayr, A., Riechelmann, D., Dietzel, M., and Schulte, U.: Magnesium-isotope fractionation during low-Mg calcite precipitation in a limestone cave - Field study and experiments. Geochim. Cosmochim. Ac. 74, 4346–4364, doi.org/10.1016/j.gca.2010.05.006, 2010.

Jex, C. N., Mariethoz, G., Baker, A., Graham, P., Andersen, M., Acworth, I., Edwards, N., and Azcurra, C.: Spatially dense drip hydrological monitoring and infiltration behaviour at the Wellington Caves, South East Australia, Int. J. Speleol., 41, 283–296, http://dx.doi.org/10.5038/1827-806X.41.2.14, 2012.

Kaushal, N., Breitenbach, S. F. M., Lechleitner, F. A., Sinha A., Tewari, V. C., Ahmad, S. M., Berkelhammer, M., Band, S., Yadava, M., Ramesh, R., and Henderson G.M.: The Indian Summer Monsoon from a Speleothem $\delta^{18}O$ Perspective – A Review, Quaternary, 1, 29, doi.org/10.3390/quat1030029, 2018.

Keller, E., Ehtesham, E., Hayman, A., Hale, R., Baisen, T., and Frew, R., NZ CDRP full isotope database, 2014.

Lechleitner, F. A., Breitenbach, S. F. M., Cheng, H., Plessen B., Rehfeld K., Goswami B., Marwan, N., Eroglu D., Adkins, J., and Haug, G. H.: Climatic and in-cave influences on $\delta^{18}O$ and $\delta^{13}C$ in a stalagmite from northeastern India through the last deglaciation. Quaternary Res. 88, 458–471, doi.org/10.1017/qua.2017.72, 2017.

Li, X., Cui, X., He, D., Liao, J., and Hu, C.: Evaluation of the Heshang Cave stalagmite calcium isotope composition as a paleohydrologic proxy by comparison with the instrumental precipitation, Sci. Rep., 8, 2615, doi.org/10.1038/s41598-018-20776-5, 2018.

Luz, B., Barkan E.: Variations of $^{17}O/^{16}O$ and $^{18}O/^{16}O$ in meteoric waters, Geochim. Cosmochim. Ac., 74, 6276–6286, doi.org/10.1016/j.gca.2010.08.016, 2010.

Magiera, M., Lechleitner F.A., Erhardt A.M., Hartland A., Kwiecien O., Cheng, H., Bradbury H. J., Turchyn A.V., Riechelmann S., Edwards L., and Breitenbach S.F.M.: Local and regional Indian Summer Monsoon precipitation dynamics during Termination II and Last Interglacial. Geophys. Res. Lett., doi: 10.1029/2019GL083721, in press.

Mahmud, K., Marienthoz, G., Baker, A., and Treble, P. C.: Hydrological characterization of cave drip waters in a porous limestone: Golgotha Cave, Western Australia, Hydrol. Earth Syst. Sci., 22, 977–988, doi.org/10.5194/hess-22-977-2018, 2018.

Markowska, M., Baker, A., Treble, P. C., Andersen, M. S., Hankin, S., Jex, C. N., Tadros, C. V., and Roach, R.: Unsaturated zone hydrology and cave drip discharge water response: Implications for speleothem paleoclimate record variability, J. Hydrol., 529,662–675, doi.org/10.1016/j.jhydrol.2014.12.044, 2015.

Mattey, D., Lowry, D., Duffet, J., Fisher, R., Hodge, E., and Frisia, S.: A 53 year seasonally resolved oxygen and carbon isotope record from a modern Gibraltar speleothem: Reconstructed drip water and relationship to local precipitation, Earth Planet. Sc. Lett., 269, 80–95, doi.org/10.1016/j.epsl.2008.01.051, 2008.

McDermott, F.: Palaeo-climate reconstruction from stable isotope variations in speleothems: a review, Quaternary Sci. Rev., 23, 901-918, doi.org/10.1016/j.quascirev.2003.06.021, 2004.

Meckler, A. N., Clarkson, M.O., Cobb, K.M., Sodemann, H., and Adkins, J. F.: Interglacial Hydroclimate in the Tropical West Pacific Through the Late Pleistocene, Science, 336, 1301-1304, https://doi: 10.1126/science.1218340, 2012.

Moerman, J. W., Cobb, K. M., Partin, J. W., Meckler, A. N., Carolin, S. A., Adkins, J. F., Lejau, S., Malang, J., Clark, B., and Tuen, A. A.: Transformation of ENSO-related rainwater to dripwater $\delta^{18}O$ variability by vadose water mixing, Geophys. Res. Lett., 41, 7907–7915, doi:10.1002/ 2014GL061696, 2014.

Mullan, B.: Effects of ENSO on New Zealand and the South Pacific. In: Braddock, D. (ed.) Prospects and needs for climate forecasting, Miscellaneous Series Royal Society of New Zealand., 34, 23–27, 1996.

Myers, C. G., Oster, J. L., Sharp, W. D., Bennartz, Kelley, N. P., Covey, A. K. and Breitenbach, S. F. M.: Northeast Indian stalagmite records Pacific decadal climate change: Implications for moisture transport and drought in India, Geophys. Res. Lett., 42, 4124–4132, doi.org/10.1002/2015GL063826, 2015.

Nelson, C. S.: Stratigraphy and sedimentology of the Te Kuiti Group in Waitomo County, South Auckland, Ph.D. Dissertation, University of Auckland, New Zealand, 1973.

NIWA: https://niwa.co.nz/climate/summaries/annual-climate-summary-2016, 2016.

NIWA: https://niwa.co.nz/climate/summaries/seasonal/summer-2016-17, 2016b.

NIWA: https://niwa.co.nz/climate/summaries/seasonal/summer-2017-18, 2018a.

NIWA: https://niwa.co.nz/climate/summaries/seasonal/autumn-2018, 2018b.

Oster, J. L., Montañez, I. P., and Kelley, N. P.: Response of a modern cave system to large seasonal precipitation variability, Geochim. Cosmochim. Ac., 91, 92–108, https://dx.doi.org/10.1016/j.gca.2012.05.027, 2012.

Owen, R.A., Day, C.C., Hu, C.-Y., Liu, Y.-H., Pointing, M. D, Blättler, C.L., and Henderson, G.M.: Calcium isotopes in caves as a proxy for aridity: Modern calibration and application to the 8.2 kyr event, Earth Planet. Sc. Lett., 443, 129–138, doi.org/10.1016/j.epsl.2016.03.027, 2016.

Riechelmann, S., Buhl, D., Schröder-Ritzrau, A., Riechelmann, D.F.C., Richter, D.K., Vonhof, H.B., Wassenburg, J., Geske, A., Spötl, C., and Immenhauser, A.: The magnesium isotope record of cave carbonate archives. Clim. Past, 8, 1849–1867, doi.org/10.5194/cp-8-1849-2012, 2012.

Risi, C., Bony, S., and Vimeux, F.: Influence of convective processes on the isotopic composition ($\delta^{18}O$ and δD) of precipitation and water vapor in the tropics: 2. Physical interpretation of the amount effect, J. Geophys. Res. 113, doi:10.1029/2008JD009943, 2008.

Schoenemann, S.W., Schauer, A.J., and Steig, E.J., Measurement of SLAP and GISP $\delta^{17}O$ and proposed VSMOW-SLAP normalization for $\delta^{17}O$ and ^{17}O-excess, Rapid Commun. Mass Sp., 27, 582–590, doi.org/10.1002/rcm.6486, 2013.

Sha, L., Mahata, S., Duan, P., Luz, B., Zhang, P., Baker, J., Zong, B., Ning, Y., Brahim, Y. A., Zhang, H., Edwards, R. L., Cheng, H.: A novel application of triple oxygen isotope ratios of speleothems, Geochim. Cosmochim. Ac., 270, 360-378, doi.org/10.1016/j.gca.2019.12.003, 2020.

Shulmeister, J., Goodwin, I., Renwick, J., Harle, K., Aremand, L., McGlone, M.S., Cook, E., Dodson, J., Hesse, P.P., Mayewski, P., and Curran, M.: The Southern Hemisphere westerlies in the Australasian sector over the last glacial cycle: a synthesis, Quaternary Res. 118–119, 23-53, doi:10.1016/S1040-6182(03)00129-0, 2004.

Sinclair, D. J., Banner, J. L., Taylor, F. W., Partin, J., Jenson, J., Mylroie, J., Goddard, E., Quinn, T., Jocson, J., and Miklavic, B.: Magnesium and strontium systematics in tropical speleothems from the Western Pacific, Chem. Geol., 294, 1–17, doi.org/10.1016/j.chemgeo.2011.10.008, 2012.

Smart, P. L. and Friederich, H.: Water movement and storage in the unsaturated zone of a maturely karstified carbonate aquifer, in: Proceedings of the conference on Environmental Problems in Karst Terranes and their Solutions, Dublin, Ohio, 59–87, 1987.

Steig, E. J., Gkinis, V., Schauer, A.J., Schoenemann, S. W., Samek, K., Hoffnagle, J., Dennis, K. J., and Tan, S.M.: Calibrated high-precision ^{17}O-excess measurements using laser-current tuned cavity ring-down spectroscopy, Atmos. Meas. Tech., 7, 2421-2435, doi.org/10.5194/amt-7-2421-2014, 2014.

Tadros, C. V., Treble, P. C., Baker, A., Fairchild, I., Hankin, S., Roach, R., Markowska, M., and McDonald, J.: ENSO–cave drip water hydrochemical relationship: a 7-year dataset from south-eastern Australia, Hydrol. Earth Syst. Sci., 20, 4625–4640, doi.org/10.5194/hess-20-4625-2016, 2016.

Treble, P. C., Fairchild, I. J., and Fischer, M. J.: Understanding climate proxies in southwest-Australian speleothems, Pages ,16, 17–19, 2008.

Tremaine, D. M. and Froelich, P. N.: Speleothem trace element signatures: A hydrologic geochemical study of modern cave dripwaters and farmed calcite, Geochim. Cosmochim. Ac., 121, 522–545, doi.org/10.1016/j.gca.2013.07.026, 2013.

Tremaine, D. M., Sinclair D. J., Stoll, H. M., Lagerström, M., Carvajal, C. P., and Sherrell, R. M.: A two-year automated dripwater chemistry study in a remote cave in the tropical south Pacific: Using [Cl–] as a conservative tracer for seasalt contribution of major cations, Geochim. Cosmochim. Ac., 184, 289–310, https://dx.doi.org/10.1016/j.gca.2016.03.029, 2016.

Uechi, Y., and Uemura, R.: Dominant influence of the humidity in the moisture source region on the ^{17}O-excess in precipitation on a subtropical island, Earth Planet. Sc. Lett., 513, 20–28, doi.org/10.1016/j.epsl.2019.02.012, 2019.

Ummenhofer, C. C. and England, M. H.: Interannual Extremes in New Zealand Precipitation Linked to Modes of Southern Hemisphere Climate Variability, J. Clim., 20, 5418-5440, https://doi.org./10.1175/2007JCLI1430.1, 2007.

Wang, Y. J., Cheng, H., Edwards, R. L., An, Z. S., Wu, J. Y., Shen, C.-C., and Dorale, J. A.: A High-Resolution Absolute-Dated Late Pleistocene Monsoon Record from Hulu Cave, China. Science, 294, 2345-2348, doi:10.1126/science.1064618, 2001.

Wang, Y. J., Cheng, H., Edwards R. L., Kong, X., Shao, X., Chen, S., Wu J., Jiang, X., Wang, X., and An Z.: Millennial-and orbital-scale changes in the East Asian monsoon over the past 224,000 years. Nature, 451, 1090-1093, https://doi.org/10.1038/nature06692, 2008.

Wassenburg, J., Immenhauser, A., Richter, D. K., Jochum, K. P., Fietzke, J., Deininger, M., Goos, M., Scholz, D., and Sabaoui, A.: Climate and cave control on Pleistocene/Holocene calcite-to-aragonite transitions in speleothems from Morocco: Elemental and isotopic evidence, Geochim. Cosmochim. Ac., 92, 23–47, doi.org/10.1016/j.gca.2012.06.002, 2012.

Williams, P.W., and Fowler, A.: Relationship between oxygen isotopes in rainfall, cave percolation waters and speleothem calcite at Waitomo, New Zealand, Journal of Hydrology (NZ), 41, 53–70, 2002.

Table 1. Summary of drip site morphological characteristics, location in the cave, response time to antecedent rainfall (values in bold were calculated from the logger records, the rest from manual drip counts), coefficient of variation % (CV), and hydrological behavior.

Drip Site	Description	Location	Height to the ceiling (m)	Mean discharge (μLs^{-1})	Response time to rainfall (days)	CV (%)	Flow pattern	Type
WP 1-1	Part of the flowstone curtain	Organ loft	6	63.35	**17**	52.9	Diffuse flow	1
WP 1-2	Part of the flowstone curtain	Organ loft	6	43.74	**15**	85.1	Diffuse flow	1
WP 1-3	Part of the flowstone curtain	Organ loft	6	105.57	**16**	56.2	Diffuse flow	1
WP 1-4	Part of the flowstone curtain	Organ loft	6	22.13	18	53.9	Diffuse flow	1
WP 1A	Part of the flowstone curtain	Organ loft	6	83.99	18	36.3	Diffuse flow	1
WP 1B	Part of the flowstone curtain	Organ loft	6	51.83	11	48.2	Combined flow	3
WP FB	Flowstone bottom	Organ loft	8	30.08	9	81.8	Diffuse flow	1
WP-2	Independent stalactite	Upper gallery	9	59.57	**4**	149.4	Fracture flow	2
WP-3	Independent stalactite	Upper gallery	9	91.62	11	31.3	Combined flow	3
WP-4	Independent stalactite	Upper gallery	12	32.07	6	53.2	Fracture flow	2

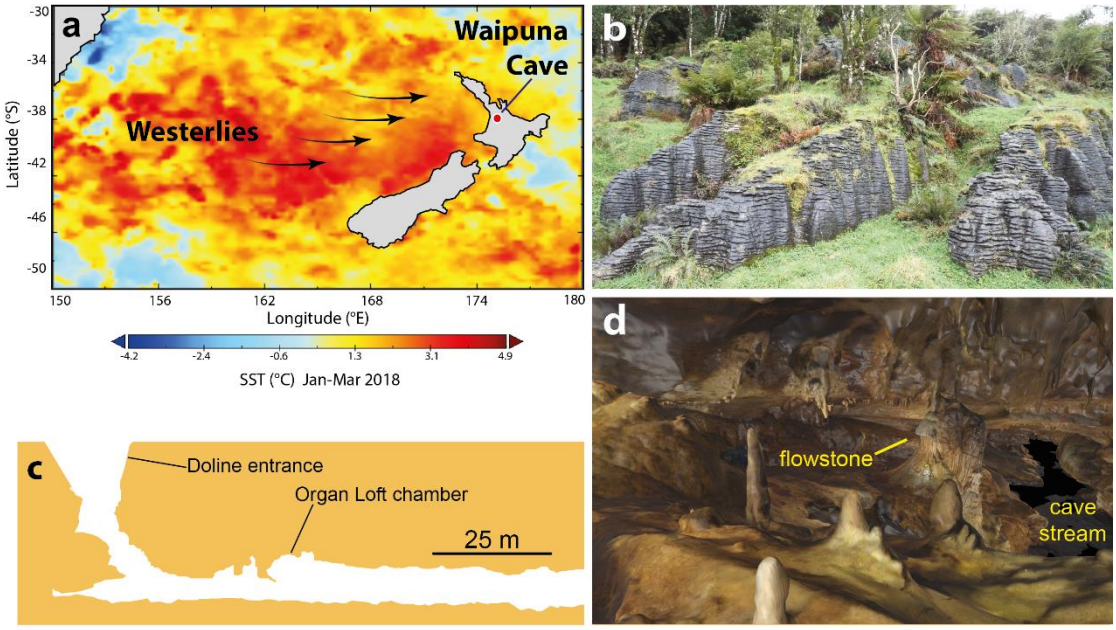

735

Figure 1. a) geographical location of Waipuna Cave and its climatic settings during La Niña conditions in summer 2018, with the direction of the Westerlies. Source data: OSTIA. b) pancake limestone outcrop landscape above Waipuna Cave. c) cross section through the entrance and first stretch of Waipuna Cave. d) 3D model of Organ Loft Chamber photo taken by John Hellstrom using structure from motion (SfM) mapping.

740

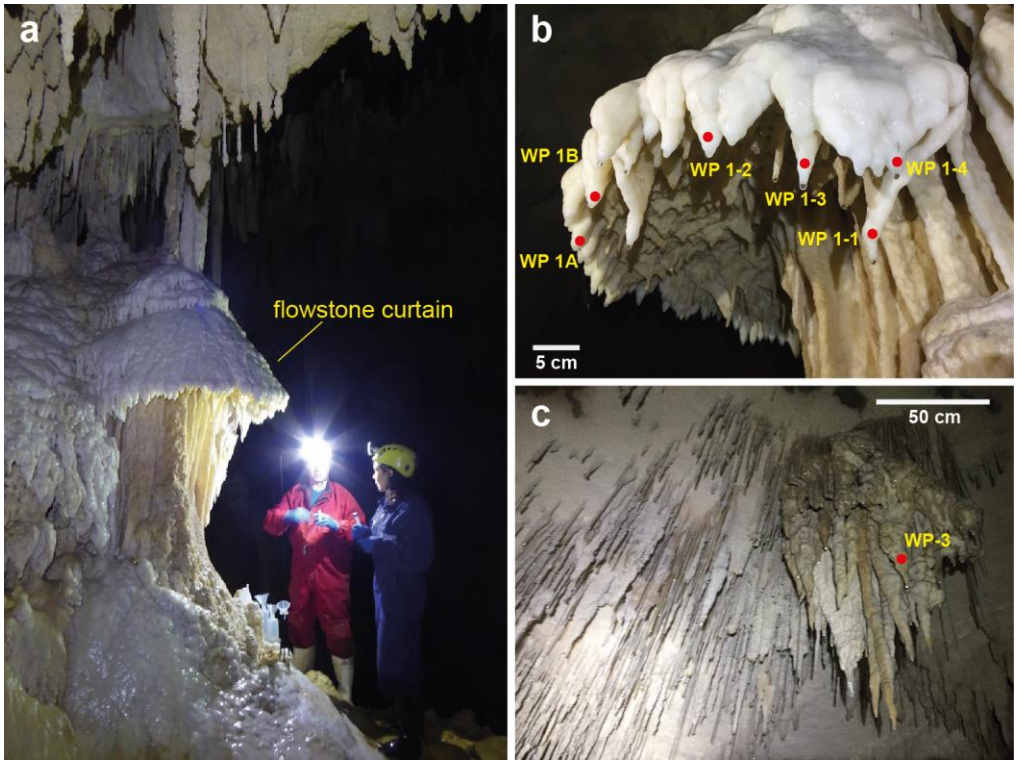

Figure 2. a) flowstone formation in the "Organ Loft" chamber (Photograph courtesy of I. Heidke). b) drip sites at the flowstone curtain. c) stalactite cluster where drip site WP-3 is located, hanging from the ceiling 6 m high in an inclined plane.

745

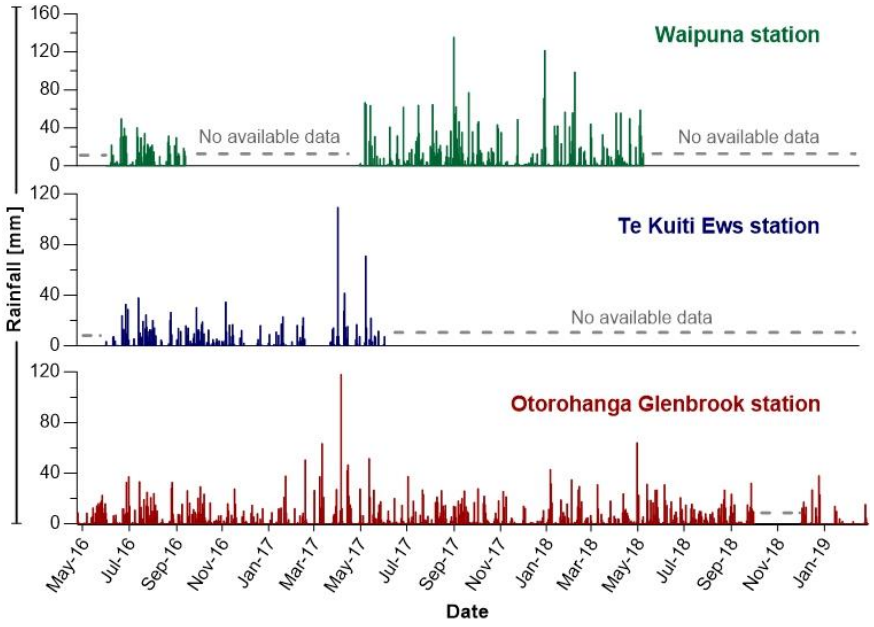

Figure 3. Daily precipitation from the Waipuna meteorological station (no data is available for October and November 2018 due to instrument failure), Otorohanga Glenbrook and Te Kuiti Ews stations (data from NIWA National Climate Database, www.clifo.niwa.co.nz).

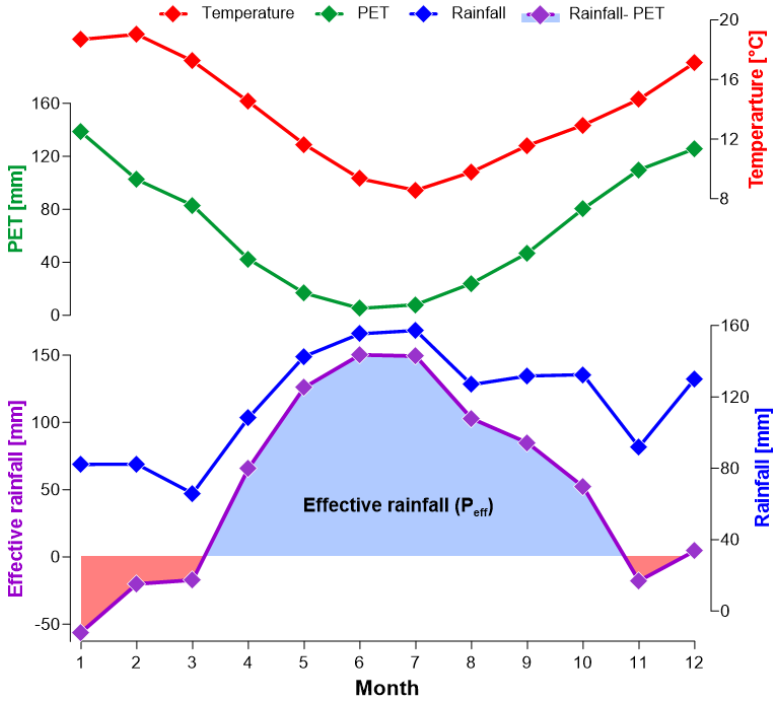

Figure 4. Mean monthly temperature (red line), precipitation (blue line), and Priestley-Taylor potential evapotranspiration (PET) recorded at Te Kuiti Ews station between 2002 and 2019 (green line) (http://cliflo.niwa.co.nz), and difference between rainfall and PET (purple line). The shaded blue area represents the effective rainfall (P_{eff}).

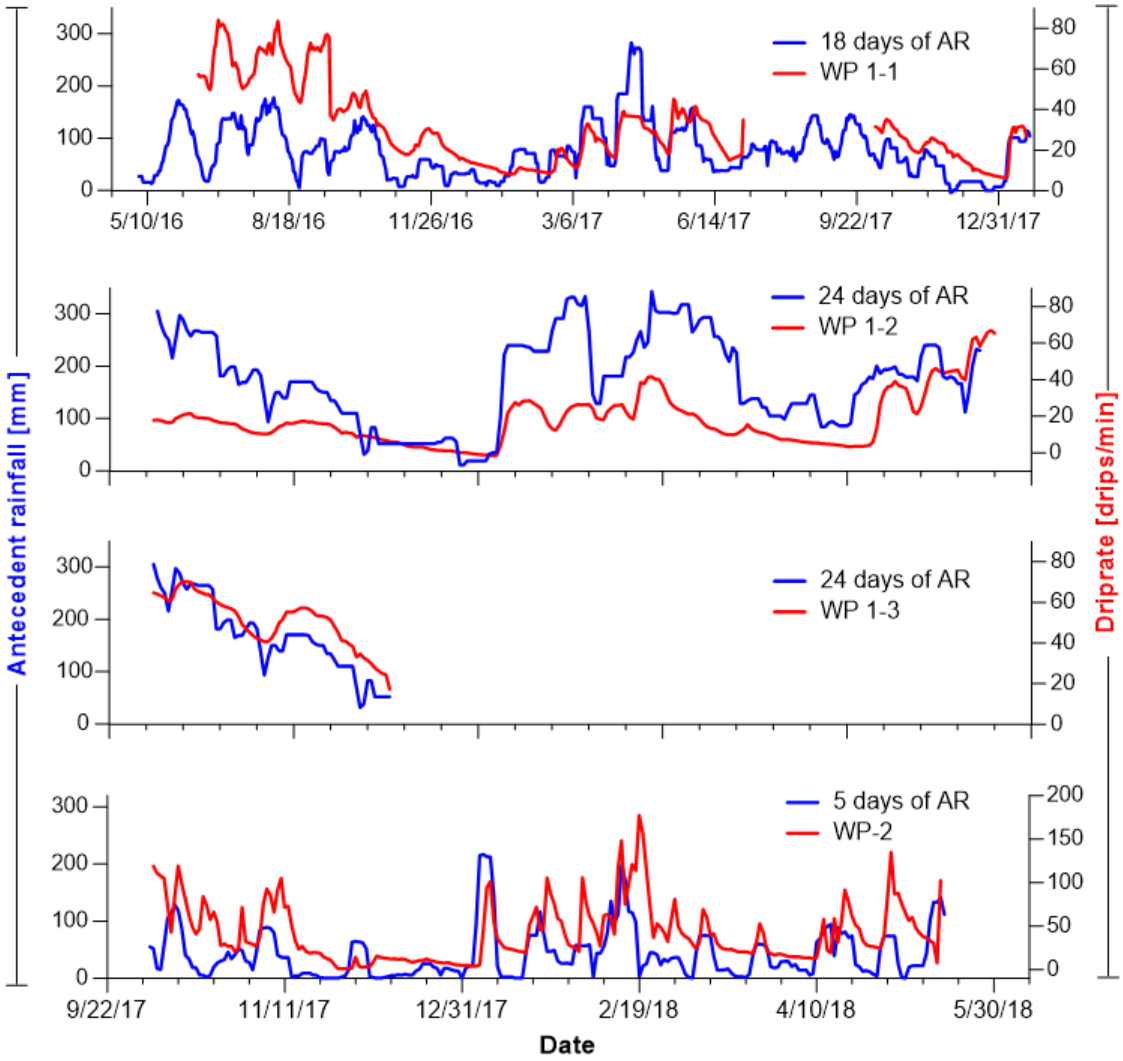

Figure 5. Drip rates recorded by the loggers (red line) for the drip sites WP 1-1, WP 1-2, WP 1-3 and WP-2, plotted with their best-fit of antecedent effective-rainfall days (blue).

760

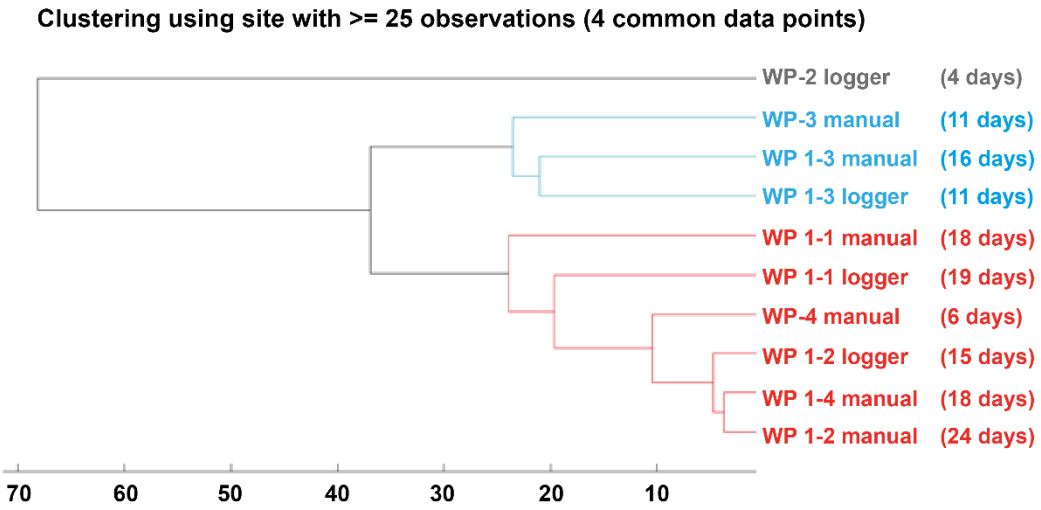

Figure 6. Results of cluster analysis of the drip site discharge time series, indicating the number of lag days calculated from the cross-correlation analysis. The gray cluster shows the drip site with the shortest lag to the antecedent rainfall (4 days), the blue 765 **cluster groups the drip sites with lag days between 11 and 16 days to antecedent rainfall, and the red cluster includes drip sites with a lag to antecedent rainfall between 15 and 24 days, with the exception of WP-4 (see main text).**

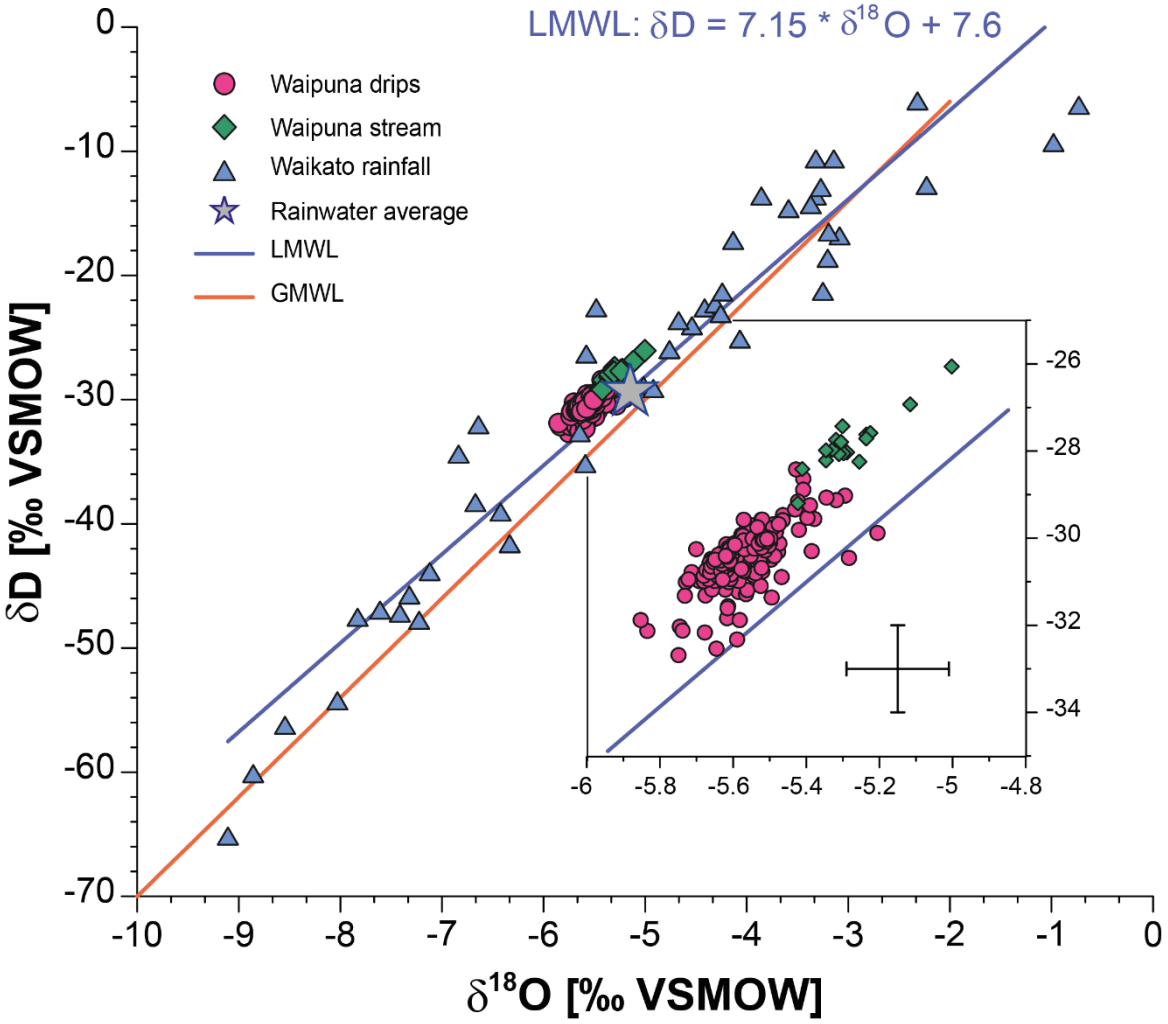

770

Figure 7. Cross-plot of δD versus $\delta^{18}O$ in dripwater (pink circles), the Waikato region precipitation (blue triangles) and Waipuna stream (green diamonds). All cave waters fall in a very narrow range (inset) and within error on the Local Meteoric Water Line (blue line, Keller et al., 2014). The cross in the inset shows the 2σ uncertainties for $\delta^{18}O$ and δD.

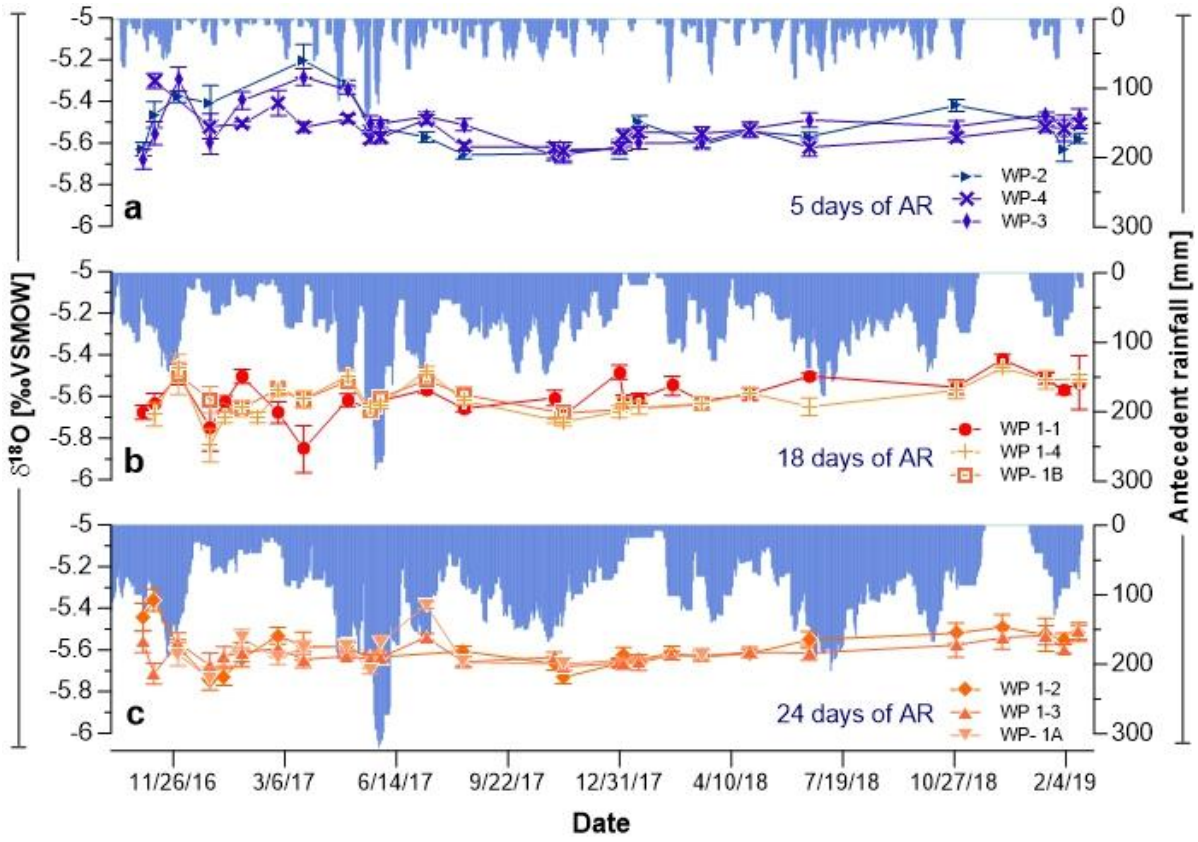

775 **Figure 8. Dripwater $\delta^{18}O$ time series of all drips grouped according to the three main response lags (5, 18, and 24 days) to antecedent rainfall (AR) at Otorohanga Glenbrook station (blue vertical bars). a) drip sites WP-2, WP-3, and WP-4 (5 days' antecedent rainfall). b) drip sites from the flowstone curtain, WP 1-1, WP 1-4 and WP 1B (18 days' antecedent rainfall). c) drip sites from the flowstone curtain WP 1-2, WP 1-3 and WP1A (24 days' antecedent rainfall). The Otorohanga rainfall record covers the period between September 2016 and January 2019; no data are available for October and November 2018.**

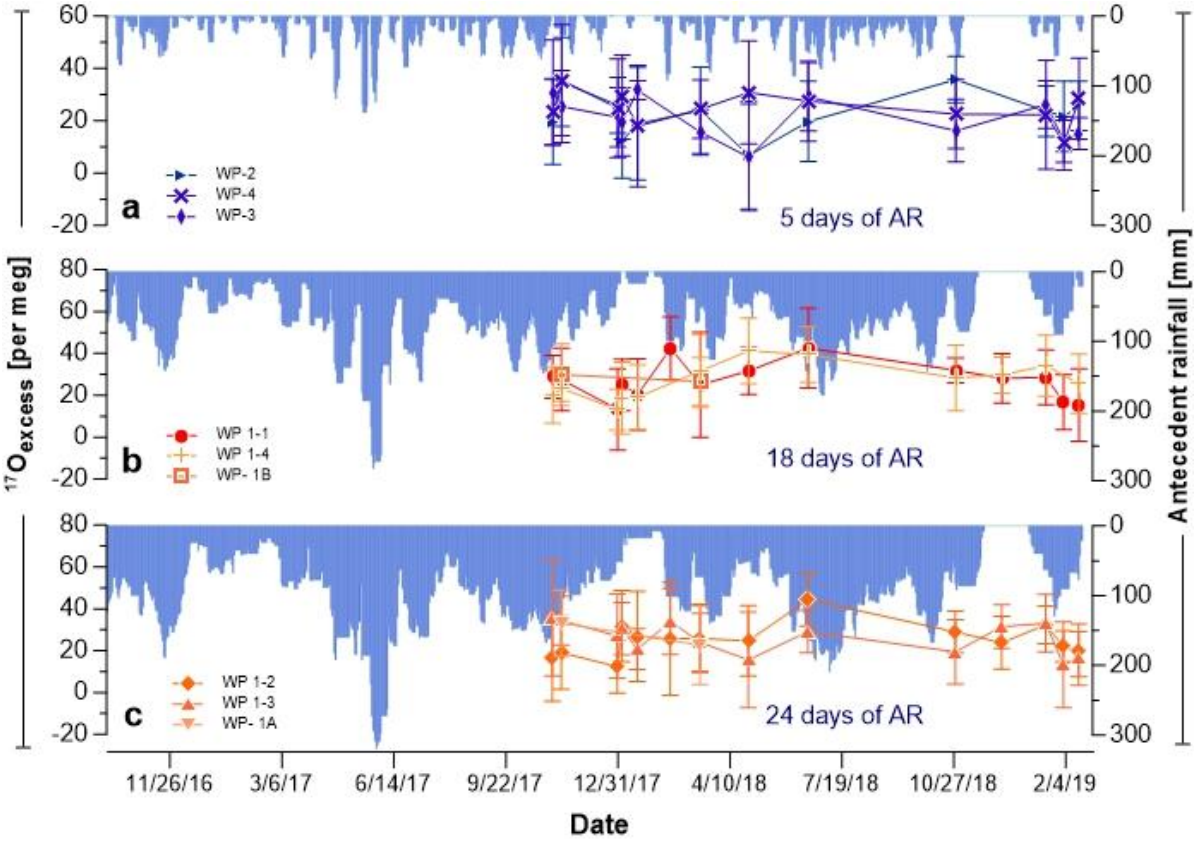

780 **Figure 9. Dripwater $^{17}O_{excess}$ time series of all drips grouped according to the three main response lags (5, 18, and 24 days) to antecedent rainfall (AR) at Otorohanga Glenbrook station (blue vertical bars). a) drip sites WP-2, WP-3, and WP-4 (5 days' antecedent rainfall). b) drip sites from the flowstone curtain, WP 1-1, WP 1-4 and WP 1B (18 days' antecedent rainfall). c) drip sites**

from the flowstone curtain WP 1-2, WP 1-3 and WP1A (24 days' antecedent rainfall). The Otorohanga rainfall record covers the period between September 2016 and January 2019; no data are available for October and November 2018.

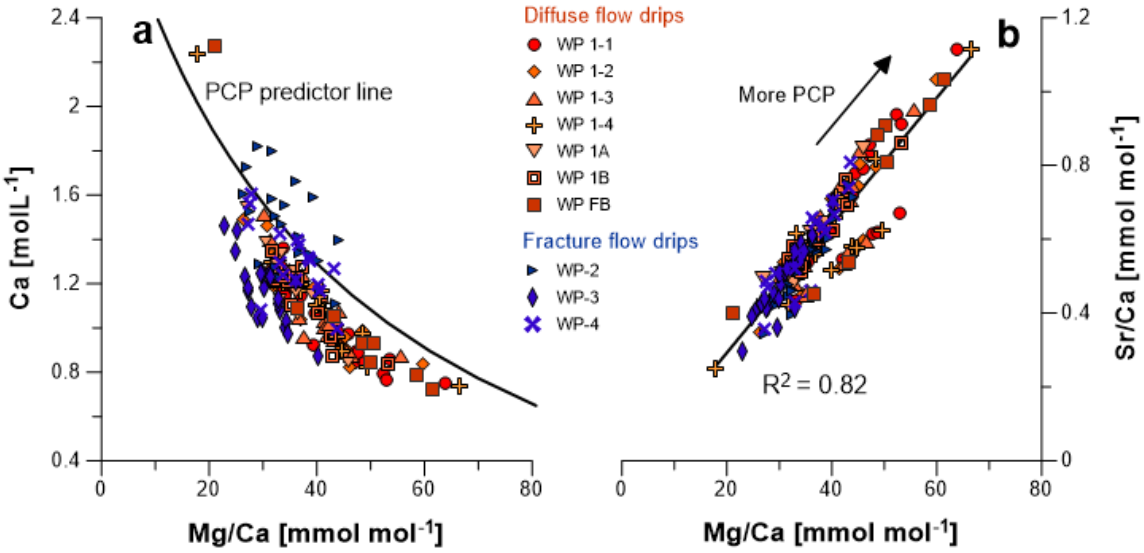

Figure 10. Waipuna Cave dripwaters sampled during the monitoring period October 2016 to January 2019. a) Ca concentration versus Mg/Ca ratios. b) Mg/Ca versus Sr/Ca, $R^2 = 0.82$, $p < 0.001$. The orange symbols correspond to diffuse flow drip sites and blue symbols signify fracture flow drip sites. The two different trends evident in the relationship between Mg/Ca and Sr/Ca will be discussed in section 5.5.

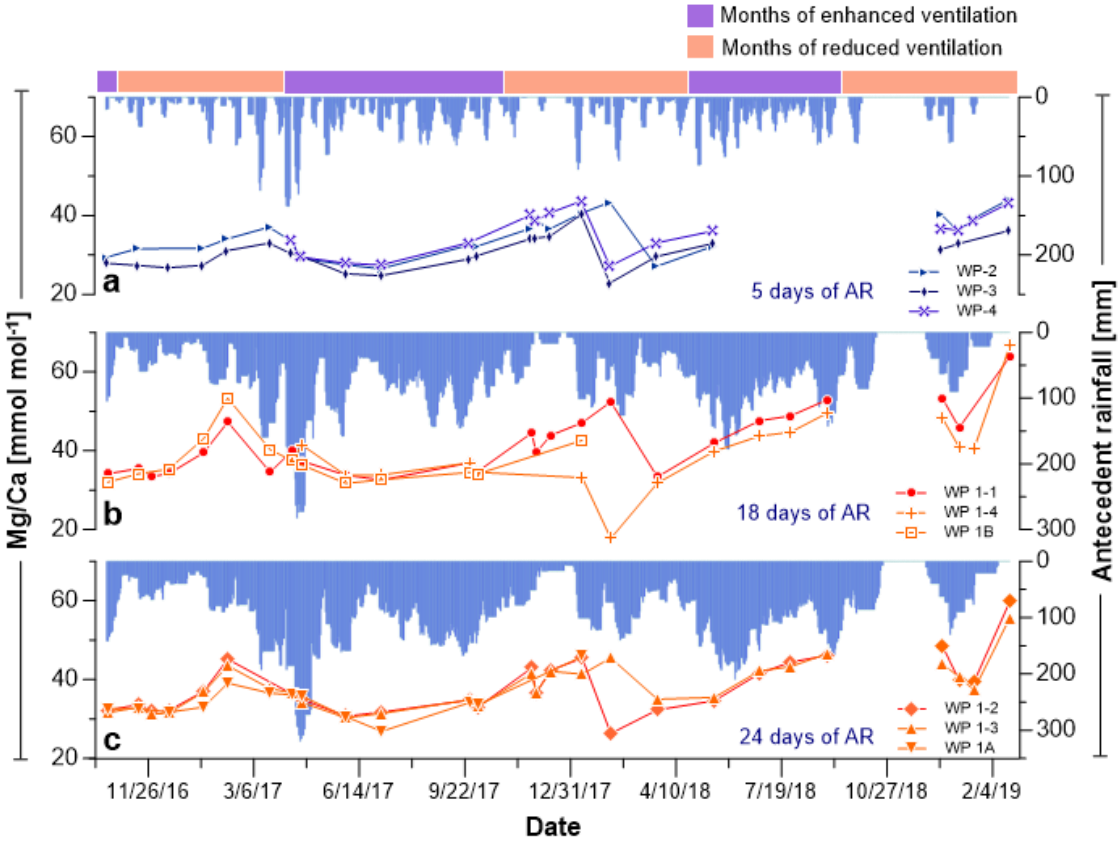

Figure 11. Dripwater Mg/Ca ratios time series of all drips grouped according to the three main response lags (5, 18, and 24 days) to antecedent rainfall (AR) at Otorohanga Glenbrook station (blue vertical bars). a) drip sites WP-2, WP-3, and WP-4 (5 days' antecedent rainfall). b) drip sites from the flowstone curtain WP 1-1, WP 1-4 and WP 1B (18 days' antecedent rainfall). c) drip sites from the flowstone curtain WP 1-2, WP 1-3 and WP1A (24 days' antecedent rainfall). The Otorohanga rainfall record covers the period between September 2016 and January 2019; no data are available for October and November 2018.

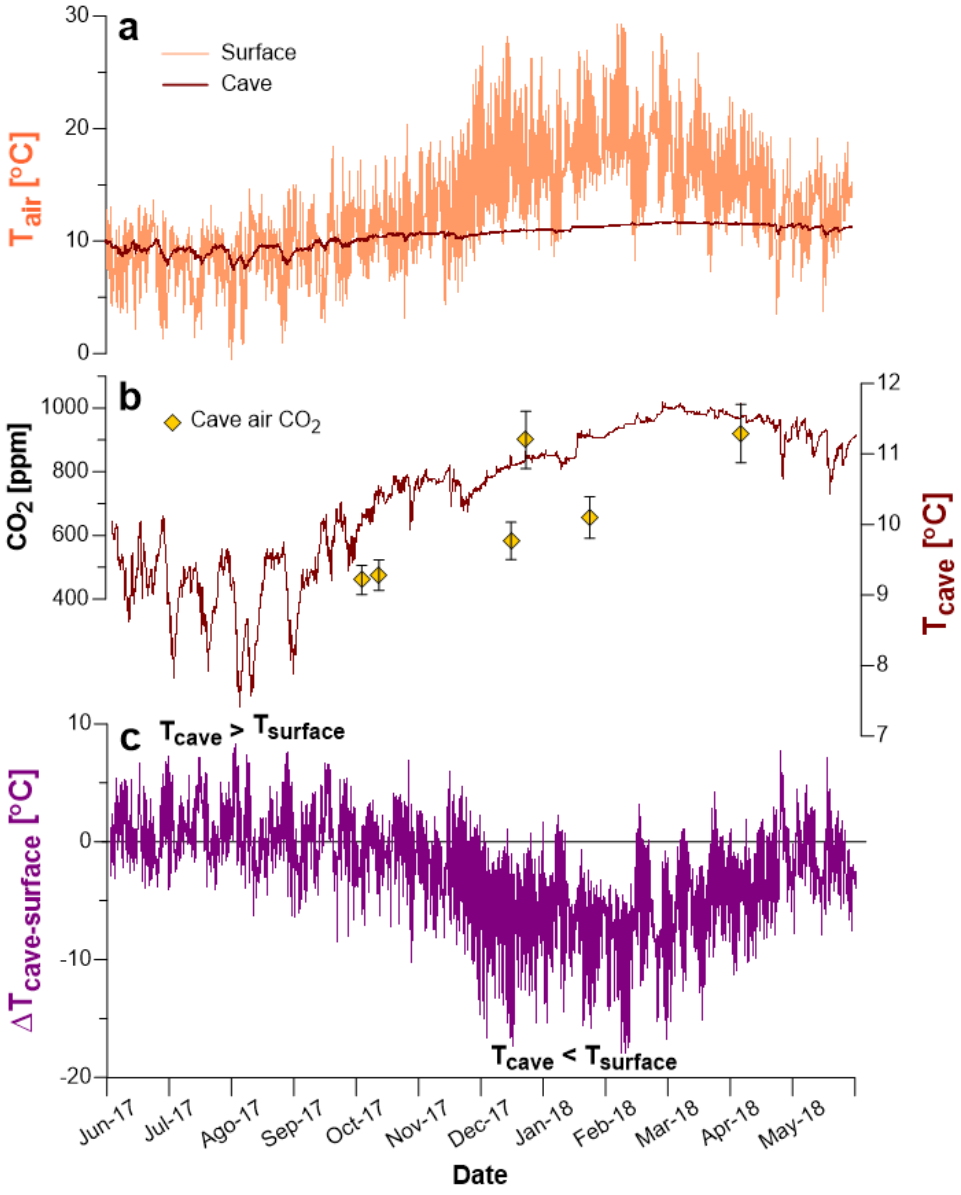

Figure 12. Comparison of meteorological parameters. a) daily mean air temperature at Waipuna station and in Waipuna Cave (in Organ Loft chamber). b) manual cave air CO_2 concentrations and daily mean air temperature in the Organ Loft chamber. c) calculated temperature difference ΔT between cave air and surface air from June to May 2018. During winter, the cave is warmer, and during summer, the cave is colder compared to the surface air.

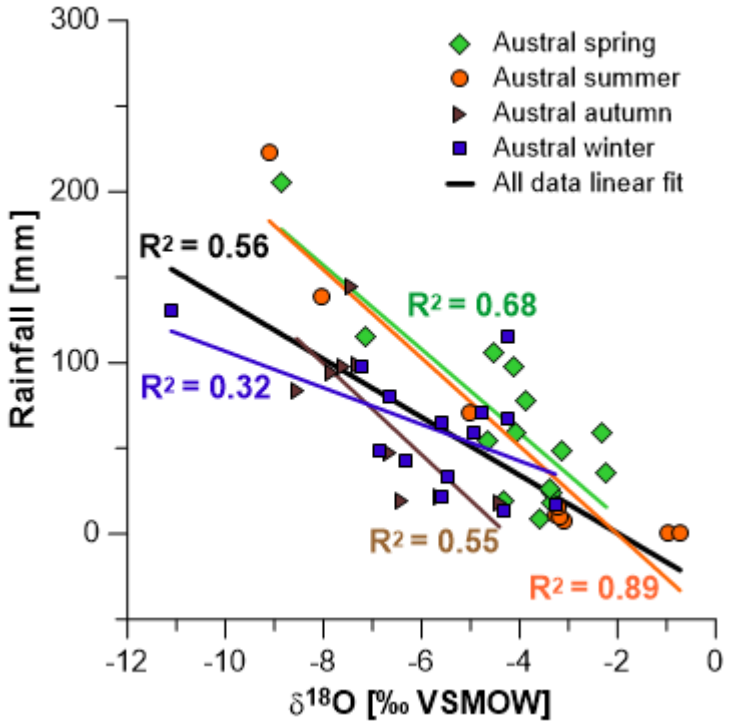

Figure 13. Cross-plot of precipitation amount versus $\delta^{18}O$ in rainfall for the period August 2007 to December 2009 from the Waikato region (Data source: Keller, 2014). The black line indicates the correlation if all data are considered, while the colored symbols and regressions relate to the different seasons.

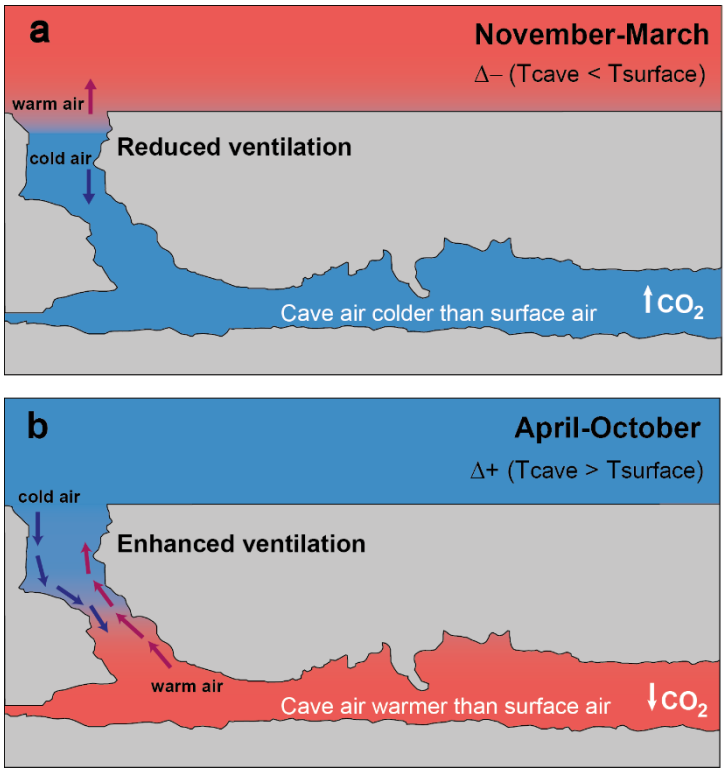

Figure 14. Conceptual model of Waipuna Cave ventilation and cave air CO_2 dynamics. The cave air is warmer in summer colder in winter. However, in summer cave air is colder than surface air (Δ+) and in winter cave air is warmer than surface air (Δ-). a) spring and summer when warmer surface conditions compared to the cave interior leads to a stagnant cold air lake and maximum CO_2 values in the cave, and b) autumn and winter conditions characterised by low surface and relatively higher cave air temperatures, facilitating barometric ventilation and exhalation of cave air CO_2 to the surface.

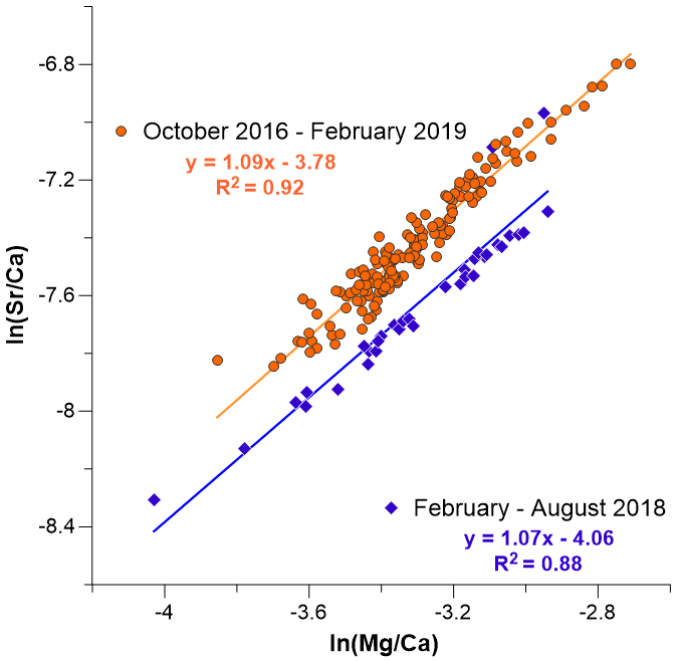

815

Figure 15. Dripwater ln(Mg/Ca) versus ln(Sr/Ca) ratios in Waipuna Cave. Blue diamonds indicate samples collected between late February 2018 to the end of August 2018, orange circles all other samples collected between October 2016 and February 2019.